Test of lepton flavor universality using $B^0 \to D^{*-}\tau^+\nu_\tau$ decays with hadronic τ channels

R. Aaij *et al.*[*]
(LHCb Collaboration)

(Received 3 May 2023; accepted 6 June 2023; published 27 July 2023)

The branching fraction $\mathcal{B}(B^0 \to D^{*-}\tau^+\nu_\tau)$ is measured relative to that of the normalization mode $B^0 \to D^{*-}\pi^+\pi^-\pi^+$ using hadronic $\tau^+ \to \pi^+\pi^-\pi^+(\pi^0)\bar{\nu}_\tau$ decays in proton-proton collision data at a center-of-mass energy of 13 TeV collected by the LHCb experiment, corresponding to an integrated luminosity of 2 fb^{-1}. The measured ratio is $\mathcal{B}(B^0 \to D^{*-}\tau^+\nu_\tau)/\mathcal{B}(B^0 \to D^{*-}\pi^+\pi^-\pi^+) = 1.70 \pm 0.10^{+0.11}_{-0.10}$, where the first uncertainty is statistical and the second is related to systematic effects. Using established branching fractions for the $B^0 \to D^{*-}\pi^+\pi^-\pi^+$ and $B^0 \to D^{*-}\mu^+\nu_\mu$ modes, the lepton universality test $\mathcal{R}(D^{*-}) \equiv \mathcal{B}(B^0 \to D^{*-}\tau^+\nu_\tau)/\mathcal{B}(B^0 \to D^{*-}\mu^+\nu_\mu)$ is calculated, $\mathcal{R}(D^{*-}) = 0.247 \pm 0.015 \pm 0.015 \pm 0.012$, where the third uncertainty is due to the uncertainties on the external branching fractions. This result is consistent with the Standard Model prediction and with previous measurements.

DOI: 10.1103/PhysRevD.108.012018

I. INTRODUCTION

Measurements of $\mathcal{R}(D^{(*)}) \equiv \mathcal{B}(B^0 \to D^{(*)}\tau^+\nu_\tau)/\mathcal{B}(B^0 \to D^{(*)}\ell^+\nu_\ell)$, the ratio of branching fractions with $\ell = \mu$, e, test lepton flavor universality in $b \to c\ell\nu_\ell$ transitions. First measured by the *BABAR* Collaboration in 2012 [1], this ratio has been studied by the Belle [2,3] and LHCb [4,5] experiments using hadronic and muonic decay modes of the τ^+ lepton.[1] After the latest LHCb Collaboration result using muonic τ^+ decays [6], the discrepancy between the world-average values of $\mathcal{R}(D^*)$ and $\mathcal{R}(D)$ measurements with their theoretical prediction is at the level of 3 standard deviations [7]. The predicted value by the Standard Model (SM) of particle physics is $R(D^*) = 0.254 \pm 0.005$ [7]. Several extensions to the SM can explain this anomaly, e.g., leptoquark models [8–10], which typically assume a leptoquark that preferentially couples to third-generation leptons and has a mass below 1 TeV/c^2.

The LHCb hadronic $\mathcal{R}(D^{*-})$ analysis was first performed using proton-proton (pp) collision data collected at center-of-mass energies of $\sqrt{s} = 7$ and 8 TeV in 2011 and 2012 [4,5], corresponding to an integrated luminosity of 3 fb^{-1}. This paper presents a similar measurement of $\mathcal{R}(D^{*-})$ based on pp collision data taken at 13 TeV in 2015 and 2016, corresponding to an integrated luminosity of 2 fb^{-1}. Despite the lower integrated luminosity, the increase of the $b\bar{b}$ production cross section with the center-of-mass energy by nearly a factor of 2 and improvements in the LHCb trigger provide about 40% more signal candidates than in the previous analysis.

The analysis strategy in this paper is similar to that detailed in the previous study [4,5], and includes changes that improve the signal efficiency. The τ^+ lepton is reconstructed in the hadronic final state $3\pi(\pi^0)\bar{\nu}_\tau$, where $3\pi \equiv \pi^+\pi^-\pi^+$, and the D^{*-} candidate is reconstructed through the $D^{*-} \to \pi^-\bar{D}^0(\to K^+\pi^-)$ decay.[2] The $B^0 \to D^{*-}3\pi$ decay is chosen as the normalization mode because it has the same visible final state as the signal mode. Many of the systematic uncertainties due to detector and reconstruction effects cancel in the ratio of their branching fractions defined as

$$\mathcal{K}(D^{*-}) \equiv \frac{\mathcal{B}(B^0 \to D^{*-}\tau^+\nu_\tau)}{\mathcal{B}(B^0 \to D^{*-}3\pi)} = \frac{N_{\rm sig}}{N_{\rm norm}}\frac{\varepsilon_{\rm norm}}{\varepsilon_{\rm sig}} \times \frac{1}{\mathcal{B}(\tau^+ \to 3\pi\bar{\nu}_\tau) + \mathcal{B}(\tau^+ \to 3\pi\pi^0\bar{\nu}_\tau)}. \quad (1)$$

Here, $N_{\rm sig}$ and $N_{\rm norm}$ are the yields in the signal and normalization modes, respectively, which are obtained from the data. The efficiencies $\varepsilon_{\rm sig}$ and $\varepsilon_{\rm norm}$, for the signal and normalization modes, respectively, are determined

[*]Full author list given at the end of the article.

[1]*BABAR* and Belle used decays with both muons and electrons in the $\mathcal{R}(D^{(*)})$ denominator, while LHCb has exclusively studied decays with muons so far.

[2]The inclusion of charge-conjugate decay modes is implied throughout the paper.

from the simulation. The signal efficiency $\varepsilon_{\rm sig}$ is calculated as the average between the $\tau^+ \to 3\pi\bar{\nu}_\tau$ and the $\tau^+ \to 3\pi\pi^0\bar{\nu}_\tau$ decays weighted by their relative branching fractions [11]. Finally, using the known branching fractions $\mathcal{B}(B^0 \to D^{*-}3\pi)$ and $\mathcal{B}(B^0 \to D^{*-}\mu^+\nu_\mu)$ [11], $\mathcal{R}(D^{*-})$ is obtained as

$$\mathcal{R}(D^{*-}) = \mathcal{K}(D^{*-}) \frac{\mathcal{B}(B^0 \to D^{*-}3\pi)}{\mathcal{B}(B^0 \to D^{*-}\mu^+\nu_\mu)}. \tag{2}$$

To avoid biases, the numerical results of this analysis were not examined until the full procedure had been finalized.

This paper is organized as follows. The LHCb detector and simulation are described in Sec. II. Details of the selection criteria used to select the $B^0 \to D^{*-}\tau^+\nu_\tau$ and $B^0 \to D^{*-}3\pi$ candidates are presented in Sec. III, followed by Sec. IV, which describes the study of the double-charm decays of the B meson that form the dominant background for the signal mode. The determination of the signal and normalization yields are provided in Sec. V, and the systematic uncertainties are discussed in Sec. VI. Finally, the results are given in Sec. VII.

II. DETECTOR AND SIMULATION

The LHCb detector [12,13] is a single-arm forward spectrometer covering the pseudorapidity range $2 < \eta < 5$, designed for the study of particles containing b or c quarks. The detector includes a high-precision tracking system consisting of a silicon-strip vertex detector surrounding the pp interaction region [14], a large-area silicon-strip detector located upstream of a dipole magnet with a bending power of about 4 Tm, and three stations of silicon-strip detectors and straw drift tubes [15,16] placed downstream of the magnet. The tracking system provides a measurement of the momentum, p, of charged particles with a relative uncertainty that varies from 0.5% at low momentum to 1.0% at 200 GeV/c. The minimum distance of a track to a primary pp collision vertex (PV), the impact parameter (IP), is measured with a resolution of $(15 + 29/p_{\rm T})$ μm, where $p_{\rm T}$ is the component of the momentum transverse to the beam, in GeV/c. Different types of charged hadrons are distinguished using information from two ring-imaging Cherenkov detectors [17]. Photons, electrons and hadrons are identified by a calorimeter system consisting of scintillating-pad and preshower detectors, an electromagnetic and a hadronic calorimeter. Muons are identified by a system composed of alternating layers of iron and multiwire proportional chambers [18].

The online event selection is performed by a trigger [19], which consists of a hardware stage based on information from the calorimeter and muon systems, followed by a software stage, which applies a full event reconstruction. At the hardware-trigger stage, events are required to have a muon with high $p_{\rm T}$ or a hadron, photon or electron with high transverse energy in the calorimeters. The hadron can originate from either the decay chain under consideration or the remainder of the event. The software trigger requires a two-, three- or four-track secondary vertex with a significant displacement from any PV. At least one charged particle must have a transverse momentum $p_{\rm T} > 1.6$ GeV/c and be inconsistent with originating from any PV. A multivariate algorithm [20,21] is used for the identification of secondary vertices consistent with the decay of a b hadron.

Simulation is required to model the effects of the detector acceptance and the imposed selection requirements. In the simulation, pp collisions are generated using PYTHIA [22] with a specific LHCb configuration [23]. Decays of unstable particles are described by EvtGen [24], in which final-state radiation is generated using PHOTOS [25]. The τ^+ decays to $3\pi\bar{\nu}_\tau$ and $3\pi\pi^0\bar{\nu}_\tau$ are simulated using the resonance chiral Lagrangian model [26] as implemented in the TAUOLA [27] package tuned according to the results from the *BABAR* Collaboration [28]. The interaction of the generated particles with the detector, and its response, are implemented using the Geant4 toolkit [29] as described in Ref. [30]. Large samples of simulated events are required to reduce the systematic uncertainty due to the sample size. A fast simulation technique, ReDecay [31], is used for this purpose in which the underlying pp interaction is reused multiple times, with an independently generated signal decay for each. These samples have been validated against simulated events using unique underlying interactions.

III. EVENT SELECTION

The reconstruction of the decay kinematics follows the procedure given in Refs. [4,5]. The signal candidates are formed by combining a D^{*-} meson that decays as $D^{*-} \to \pi^-\bar{D}^0(\to K^+\pi^-)$ and a 3π system which is detached from the B^0 decay vertex due to the non-negligible lifetime of the τ^+ lepton. The dominant background contribution is B^0 decays in which the 3π system comes promptly from the B^0 vertex, called prompt background hereafter. To suppress this background, the distance between the B^0 and 3π vertices along the beam direction, $\Delta z \equiv z(3\pi) - z(B^0)$, is required to be at least twice its uncertainty ($\sigma_{\Delta z}$). Double-charm $B \to D^{*-}D(X)$ decays[3] are the next dominant background, with a detached-vertex topology similar to that of the signal decays. The remaining sources of background are suppressed by requiring the 3π system to be consistent with originating from a common vertex.

Three categories of data and simulation are used in this analysis: signal, normalization and control. The control

[3]Throughout the paper, X denotes unreconstructed particles that are known to be present in the decay chain, and (X) stands for those that may or may not be present.

samples are used to study the double-charm background and are selected to enrich the number of D_s^+ decays. The selection process for each set is split into two stages. First, common selection criteria are applied to suppress the candidates originating from random combinations of final-state particles for the signal, normalization and control samples. Second, specific requirements are placed on each set. The selection of control samples is described in Sec. IV.

A. Common selection criteria

The purpose of these common requirements is to suppress the prompt and combinatorial backgrounds. Tracks consistent with a kaon or pion hypothesis and having $p > 2$ GeV$/c$ and $p_{\mathrm{T}} > 250$ MeV$/c$ are selected to form $\bar{D}^0$ candidates, which are required to have a mass in the range $[1840, 1890]$ MeV$/c^2$ and p_{T} larger than 1.2 GeV$/c$. The $\bar{D}^0$ candidates are then combined with tracks consistent with the pion hypothesis and with $p_{\mathrm{T}} > 110$ MeV$/c$ to form D^{*-} candidates, where the difference in the masses of the D^{*-} and $\bar{D}^0$ candidates (Δm) must lie within 143 and 148 MeV$/c^2$. Sideband regions of $m(\bar{D}^0)$ in ranges $[1825, 1840]$ MeV$/c^2$ and $[1890, 1905]$ MeV$/c^2$ and Δm within $[150, 160]$ MeV$/c^2$ are defined to study the combinatorial background.

The τ^+ candidates are formed from three tracks, where each track must have $p_{\mathrm{T}} > 250$ MeV$/c$ and be consistent with the pion hypothesis. Additionally, the 3π vertex must be separated from the PV associated with the signal decay by at least 10 times the uncertainty on the distance of separation. The radial distance between the 3π vertex and the beam center in the transverse plane is required to be within [0.2, 5.0] mm to avoid pion triplets coming from secondary interactions or a PV. The combinatorial background is suppressed by requiring that the $\bar{D}^0$ and τ^+ candidates are associated with the same PV. For events with B^0 mass greater than 5150 MeV$/c^2$, the significance of the IP of the $\bar{D}^0$ and 3π candidates with respect to the PV associated with the signal decay is required to be larger than 4.

1. Particle identification requirements

The charged pion and kaon tracks must be positively identified using the information provided by the particle identification (PID) system. The requirements are the same as those used in the previous analysis [4,5]. Contamination due to decays of the type $B \to D^{*-}D^+(X)$, with the subsequent decay $D^+ \to K^-\pi^+\pi^+(\pi^0)$, are suppressed by requiring that the kaon identification probability is less than 17% for the π^- candidate within the 3π system.

2. Anticombinatorial and isolation requirements

The combinatorial background is further suppressed using a boosted decision tree (BDT) classifier that is trained using simulated $B^0 \to D^{*-}\tau^+\nu_\tau$ decays as the signal proxy and the data sample with the same-sign charge combination $D^{*-}\pi^-\pi^+\pi^-$ as the background proxy. The distributions of p_{T} and η of the D^{*-} and τ^+ candidates along with variables related to their vertex and IP are used to separate signal and background events. Two such variables are χ^2_{IP}, which is defined as the difference in the vertex-fit χ^2 of the PV reconstructed with and without the particle under consideration, and vertex χ^2, which describes the quality of a vertex. The flight direction information of the B^0 and τ^+ is also utilized. The BDT classifier rejects about 75% of the combinatorial background while preserving 77% of the $B^0 \to D^{*-}\tau^+\nu_\tau$ decays.

A closely related challenge is the rejection of partially reconstructed backgrounds with more than six charged tracks. The main source of these candidates is $B \to D^{*-}D_s^+(X)$ processes where the D_s^+ meson decays into five stable charged particles and $B \to D^{*-}D^0K^+$ decays where the D^0 meson decays into four stable charged particles. A dedicated algorithm [32] is used to evaluate the isolation of each signal-candidate track from other nonsignal tracks in an event. An isolation BDT classifier is formed from this information for each signal-candidate track, trained using simulated $B^0 \to D^{*-}\tau^+\nu_\tau$ decays as the signal proxy and simulated $B \to D^{*-}D^0K^+$ decays in which two extraneous charged kaons are present as the background proxy. This classifier removes 82% of background decays with extra charged tracks while retaining 78% of signal decays. The isolation requirements for suppressing background with extra neutral particles in the final state are discussed in Sec. III B 2.

B. Selection of signal-mode $B^0 \to D^{*-}\tau^+\nu_\tau$

The signal-mode $B^0 \to D^{*-}\tau^+\nu_\tau$ candidates are identified with the use of a detached-vertex criterion and a targeted suppression of backgrounds where D_s^+ decays mimic hadronic decays of τ^+ leptons.

1. Vertex detachment criteria

In $B^0 \to D^{*-}\tau^+\nu_\tau$ decays, the 3π vertex is detached from the B^0 vertex. A good approximation for the B^0 vertex is the point of closest approach between the D^{*-} line of flight and the 3π line of flight. A BDT classifier is used to identify this detached topology. The inputs to this BDT classifier are the positions of the $\bar{D}^0$, B^0 and 3π vertices and their related uncertainties, the 3π mass, and the momenta of the tracks forming the B^0 candidate. The training of this BDT is performed using simulated $B^0 \to D^{*-}\tau^+\nu_\tau$ decays as signal and simulated prompt $b\bar{b} \to D^{*-}3\pi X$ production as background samples. The efficiency and rejection performance of this BDT classifier is slightly better than the beam-direction significance used in Refs. [4,5]; the rejection rate is 20% higher for the same signal efficiency.

2. Suppression of D_s^+ backgrounds

The 3π decay of the τ^+ proceeds predominantly through an a_1 resonance with a $\rho^0\pi^+$ intermediate state. There is a major background contribution due to D_s^+ decays to $3\pi(X)$, which primarily proceeds through η and η' resonances, with only a very small contribution from Ra_1 structures, where R designates an η, η', ω, ϕ or K^0 meson [11]. In addition, for the latter three mesons, the phase space is such that the a_1 meson must be produced below its on-shell mass, providing further discrimination with respect to τ decays. The $\pi^+\,\pi^-$ mass is kinematically limited to $< 400\ \mathrm{MeV}/c^2$ for the decays $\eta \to \pi^+\pi^-\pi^0$ and $\eta' \to \pi^+\pi^-\eta$, which provides input to a discriminating variable formed by the minimum mass of the two $\pi^+\,\pi^-$ combinations present in the pion triplet. The 3π system from D_s^+ decays is often accompanied with a large number of neutral particles from the same decay. Variables related to the energy from these neutral particles in cones around the 3π system direction are used in a BDT classifier to suppress these backgrounds. This classifier is trained using simulated $B^0 \to D^{*-}\tau^+\nu_\tau$ events as the signal training sample and simulated D_s^+ events decaying into three pions as the background training sample. The performance of this anti-D_s^+ BDT is better than that found in the previous analysis [4,5] with 40% rejection of D_s^+ events for a 97% signal efficiency. The anti-D_s^+ BDT output is used as a fit variable to estimate the yield of $B^0 \to D^{*-}\tau^+\nu_\tau$ decays.

3. Other requirements

The invariant mass of the 3π system is required to be below $1600\ \mathrm{MeV}/c^2$ to suppress double-charm backgrounds. An upper boundary for the invariant mass of the $D^*3\pi$ candidates is set at $5100\ \mathrm{MeV}/c^2$, consistent with the presence of neutrinos in the final state of the signal decays. After all the selection requirements are applied, only 0.5% of events have multiple candidates, from which one is chosen at random.

C. Selection of normalization mode $B^0 \to D^{*-}3\pi$

The selection of $B^0 \to D^{*-}3\pi$ candidates utilizes the unique characteristics of this mode: the fully reconstructed $B^0 \to D^{*-}3\pi$ decay and the 3π system coming directly from the B^0 meson. The B^0 candidates are selected in the mass range $[5150, 5400]\ \mathrm{MeV}/c^2$. The selection is kept similar to that of the $B^0 \to D^{*-}\tau^+\nu_\tau$ mode, to cancel the majority of systematic bias in the measurement of the ratio $\mathcal{K}(D^{*-})$. To ensure this, the $\bar{D}^0$ decay vertex is required to lie further downstream than the 3π vertex, a similar detachment criterion to that for the 3π system from the B^0 decay vertex in $B^0 \to D^{*-}\tau^+\nu_\tau$ decays. The anti-D_s^+ BDT classifier and $m(3\pi)$ selection criteria are not applied; however these do not bias $\mathcal{K}(D^{*-})$, since their efficiency is around 97% for the $B^0 \to D^{*-}\tau^+\nu_\tau$ decays.

D. Simulation corrections and efficiencies

The simulation samples used in the analysis are required to match the conditions in data as closely as possible. The p_{T} and η distributions of the B meson, $B^0 \to D^{*-}\tau^+\nu_\tau$ form factors, 3π vertex-position uncertainty and the 3π decay dynamics in simulation are calibrated to data. Control samples are used to validate simulation samples and apply corrections where necessary, as described in Sec. IV. The selection efficiencies (ε) for the $B^0 \to D^{*-}\tau^+\nu_\tau$ and $B^0 \to D^{*-}3\pi$ modes are estimated from simulation after corrections are applied. The efficiencies used in Eq. (1) are $\varepsilon_{\mathrm{sig}} = (1.05 \pm 0.01) \times 10^{-4}$ and $\varepsilon_{\mathrm{norm}} = (3.00 \pm 0.03) \times 10^{-4}$. The uncertainties are due to the limited size of the simulation samples.

IV. STUDY OF DOUBLE-CHARM BACKGROUND

The dominant background category after applying the selection criteria mentioned in Sec. III is double-charm decays $B \to D^{*-}D(X)$, where D is a D_s^+, D^+ or D^0 meson. Control samples in data are used to study these backgrounds and evaluate corrections that must be applied to simulated samples which are used to obtain the background probability density functions (PDFs) used in the fit to determine the signal yield. The decays involving D_s^+ mesons are analyzed in two stages. First, the corrections to the branching fractions used to generate the simulation of different D_s^+ decays with three pions in the final state are estimated. These corrections are applied to the simulation samples. Second, the composition of several $B \to D^{*-}D_s^+(X)$ decays is determined, serving as constraints on the fractions of these components in the signal-extraction fit.

A. $D_s^+ \to 3\pi X$ decay model

The decays of D_s^+ mesons and τ^+ leptons to final states involving three pions are distinct, as discussed in Sec. III B 2. However, the D_s^+ meson can decay to the ρ^0 meson via an η' resonance, which decays to the $\rho^0\gamma$ final state. Consequently, the ρ^0 contribution from the D_s^+ decay could be mistakenly attributed to that from a τ^+ decay. Therefore, it is crucial that contributions from various resonances, especially η', are correctly normalized in simulation to reflect the data as closely as possible. It is also essential to constrain the relative contributions of certain decay modes, whose branching fractions are not precisely measured.

The fractions of different $D_s^+ \to 3\pi X$ decays are determined from a data sample enriched in these decays. This sample is selected with the same criteria as for $B^0 \to D^{*-}\tau^+\nu_\tau$ decays but with a reverse requirement on the anti-D_s^+ BDT output. A simultaneous binned maximum-likelihood fit is performed to the distribution of four variables: $\min[m(\pi^+\pi^-)]$, $\max[m(\pi^+\pi^-)]$, $m(\pi^+\pi^+)$, which

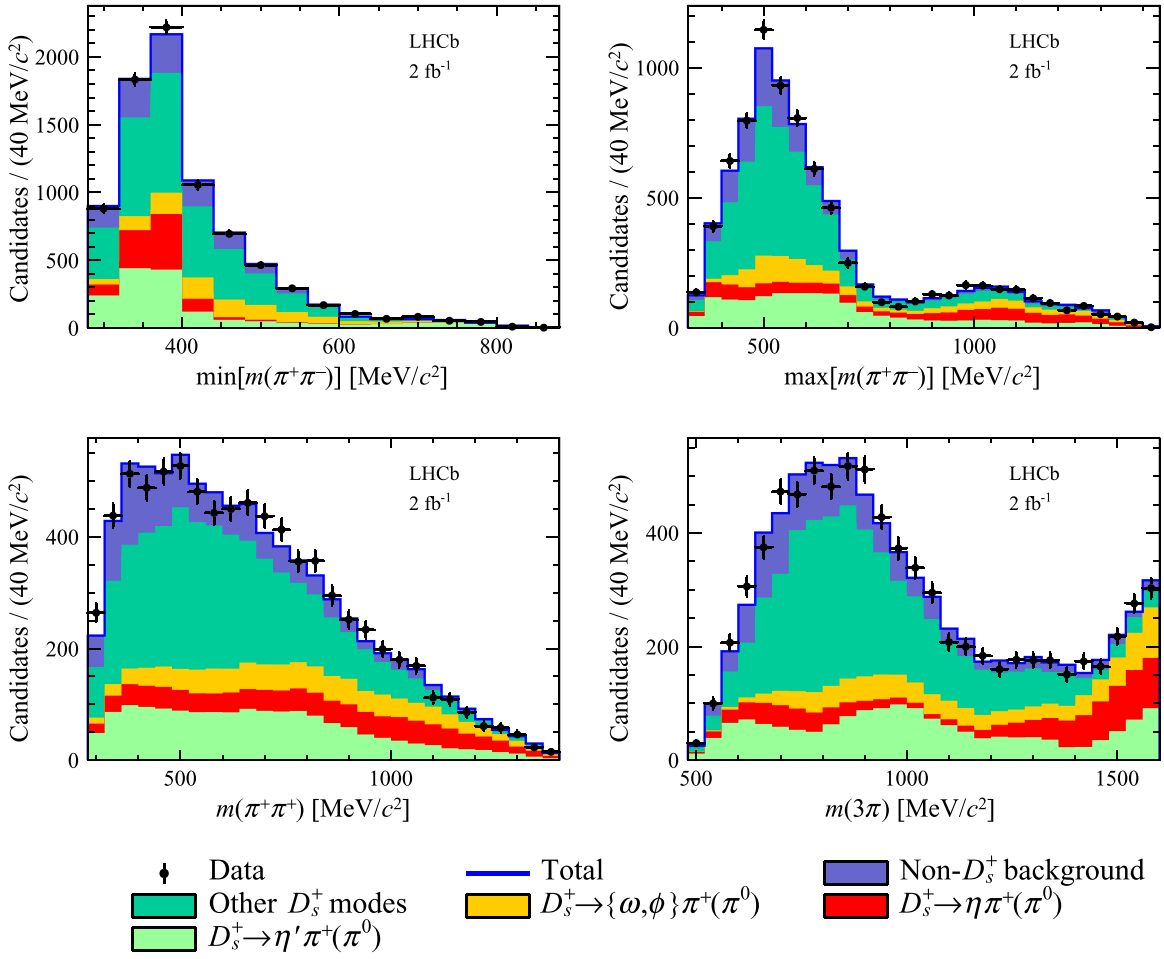

FIG. 1. Projections of the $D_s^+ \to 3\pi X$ components for the variables: $\min[m(\pi^+\pi^-)]$, $\max[m(\pi^+\pi^-)]$, $m(\pi^+\pi^+)$ and $m(3\pi)$ in the fit to the control data samples.

represents the reconstructed masses of all possible two-pion combinations of the candidate, and $m(3\pi)$. This last variable allows the exclusive $D_s^+ \to 3\pi$ decay to be distinguished from candidates where energy is carried by additional neutral particles, e.g., $D_s^+ \to \tau^+(\to 3\pi\bar{\nu}_\tau)\nu_\tau$ or $D_s^+ \to 3\pi X$, where X escapes detection.

The different D_s^+ decay components are broadly divided into four categories:

(i) $D_s^+ \to \eta\pi^+(\pi^0)$ decays where charged pions from the η meson are selected.
(ii) $D_s^+ \to \eta'\pi^+(\pi^0)$ decays where charged pions from the η' meson are selected.
(iii) $D_s^+ \to \omega\pi^+(\pi^0)$ or $D_s^+ \to \phi\pi^+(\pi^0)$ decays where charged pions from the ω or ϕ meson are selected.
(iv) D_s^+ decays where the pions originate either directly from the D_s^+ decay or from the a_1 resonance $\eta 3\pi$, ηa_1, $\eta' 3\pi$, $\eta' a_1$, $\omega 3\pi$, ωa_1, $\phi 3\pi$, ϕa_1, $K^0 3\pi$, $K^0 a_1$, $\tau^+\nu_\tau$ and nonresonant 3π.

The template PDFs for the various D_s^+ decay components are defined using inclusive $B \to D^{*-}D_s^+X$ simulation samples, and the non-D_s^+ decays are modeled using the inclusive $B \to D^{*-}3\pi X$ simulation sample. The fraction of each of the four D_s^+ decay components, relative fractions of $\eta 3\pi$, $\eta' 3\pi$ and $\omega 3\pi$ final states and the total number of D_s^+ and non-D_s^+ decays are free parameters in the fit. Compared to the previous analysis [4,5], the simulated samples are improved with the addition of $D_s^+ \to Ra_1$ modes with $R \in \{\eta, \eta', \omega, \phi, K^0\}$, which enable a more detailed description of the $D_s^+ \to 3\pi X$ decay. This introduces more fit parameters and hence additional constraints are applied to ensure the stability of the fit. The fit assumes no interference effects, as a full amplitude analysis is beyond the scope of this study. The fit results are given in Fig. 1, which shows the fractions of the four inclusive categories mentioned above. The relative fraction of the component with the π^0 meson with respect to the total fraction of each of the first three categories are Gaussian constrained around the expected value of $2/3$ with a standard deviation of 0.2. For each resonance R, the sum of $D_s^+ \to Ra_1$ and $D_s^+ \to R3\pi$ is measured. The relative fraction $D_s^+ \to Ra_1/(D_s^+ \to Ra_1 + D_s^+ \to R3\pi)$ is fixed at 5.5%. This is chosen since it provides the best quality for the signal fit. The fractions of D_s^+ decays

TABLE I. Relative fractions of various $D_s^+ \to 3\pi X$ decays obtained from the fit to the D_s^+ control sample (see Fig. 1) before applying any bias correction to the mean value of its uncertainty.

Template	$D_s^+ \to 3\pi X$ fraction
$\eta\rho^+$	0.112 ± 0.020
$\eta\pi^+$	0.021 ± 0.008
$\eta'\rho^+$	0.185 ± 0.016
$\eta'\pi^+$	0.051 ± 0.014
$\omega\rho^+$ or $\phi\rho^+$	0.090 ± 0.029
$\omega\pi^+$ or $\phi\pi^+$	0.041 ± 0.008
$\eta 3\pi$	0.081 ± 0.024
$\eta' 3\pi$	0.000 ± 0.005
$\omega 3\pi$	0.032 ± 0.041
$\phi 3\pi$	0.029 ± 0.008
$K^0 3\pi$	0.011 ± 0.003
$\tau^+\nu_\tau$	0.012 ± 0.003
Nonresonant 3π	0.326 ± 0.046
$a_1\eta$	0.005 ± 0.001
$a_1\eta'$	0.000 ± 0.001
$a_1\omega$	0.002 ± 0.002
$a_1\phi$	0.002 ± 0.001
$a_1 K^0$	0.001 ± 0.001

to $\phi a_1 + \phi 3\pi$, $K^0 a_1 + K^0 3\pi$ and $\tau^+\nu_\tau$ final states are fixed according to their known branching fractions [11].

The χ^2 per degree of freedom is evaluated to be 1.5, indicating a reasonable fit quality. Possible effects from mismodeling of the components in the fit are considered as sources of systematic uncertainties, which are described in Sec. VI. The determined fractions of the different modes are given in Table I. They are used to correct the corresponding modes in the simulation sample. The uncertainties obtained from the fit could be underestimated due to the statistical correlations arising from simultaneously fitting to four one-dimensional distributions. The effect of the correlations is investigated using a set of pseudodata samples built via bootstrapping from simulation, in which events are assigned to each component category randomly. The statistical uncertainty on the fit parameters is found to be underestimated by no more than 40%. The uncertainties of the fit parameters are then corrected according to this estimation. The correction factors are applied to the simulation samples that are used to produce the template PDFs for $B \to D^{*-} D_s^+ X$ backgrounds.

B. $B \to D^{*-} D_s^+ (X)$ control sample

The relative abundance of different $B \to D^{*-} D_s^+ (X)$ decays provides important constraints in the signal fit. These relative fractions are determined from a fit to the data control sample enriched in $B \to D^{*-} D_s^+ (\to 3\pi)(X)$ decays. The selection of the control sample differs from the default selection by requiring the 3π mass to be within 20 MeV/c^2 of the known D_s^+ mass and omitting the anti-D_s^+ BDT cut, as well as the B^0 and τ^+ mass constraints. This sample comprises modes that can be grouped into the exclusive $B^0 \to D^{*-} D_s^{(*,**)+}$ decays, and the inclusive $B \to \bar{D}^{**} D_s^+ (X)$ and $B_s^0 \to D^{*-} D_s^+ (X)$ decays.[4]

The $q^2 \equiv (p_{B^0} - p_{D^{*-}})^2$ distribution for exclusive modes peaks at the mass of the relevant $D_s^{(*,**)+}$ states, where p_H is the momentum of particle H. The inclusive $B \to D^{*-} D_s^+ X$ modes often have at least one extra particle, possibly from $\bar{D}^{**} D_s^+ (X)$ final states. These additional particles carry momentum that contributes to the q^2, shifting this distribution to higher values.

An extended binned maximum-likelihood fit is performed to the distribution of the difference of the $D^{*-} 3\pi$ mass and the sum of the reconstructed $\bar{D}^0$ and 3π masses, i.e., $\Delta M_{D^* D_s} \equiv m(D^{*-} 3\pi) - m(\bar{D}^0) - m(3\pi)$. The total PDF used in the fit is

$$\mathcal{P} = f_{\rm comb} \mathcal{P}_{\rm comb} + \frac{(1 - f_{\rm comb})}{k} \sum_i f_i \mathcal{P}_i, \qquad (3)$$

where $f_{\rm comb}$ is the fraction of the combinatorial background and $\mathcal{P}_{\rm comb}$ is the corresponding PDF that is modeled using the same-sign $D^{*+} 3\pi$ data sample, f_i are floating fractions of the different $B \to D^{*-} D_s^+ (X)$ components with $i \in \{D_s^+, D_{s0}^{*+}, D_{s1}^+, \bar{D}^{**} D_s^+ (X), B_s^0 \to D^{*-} D_s^+ (X), D_s^{*+}\}$, relative to the most abundant $B^0 \to D^{*-} D_s^{*+}$ decays, and $k = 1 + \sum_i f_i$ by definition. Here, D_{s0}^{*+} and D_{s1}^+ denote the $D_{s0}^*(2317)^+$ and $D_{s1}(2460)^+$ states, respectively. The template shape of each component is taken from simulation.

The distributions of $\Delta M_{D^* D_s}$, q^2, decay time of the τ^+ candidate (t_τ) and anti-D_s^+ BDT output are shown in Fig. 2. The fit quality is good with a χ^2 per degree of freedom equaling 1.11. The fractions of different decays are given in Table II, which are used as Gaussian constraints in the signal-extraction fit for the corresponding components after accounting for the efficiency differences between the control and signal samples.

C. $B \to D^{*-} (D^0, D^+)(X)$ control samples

The $B \to D^{*-} D^+ (X)$ and $B \to D^{*-} D^0 (X)$ decays are the subleading double-charm backgrounds in the signal sample, where the D^0 mesons decay to three charged pions plus extra particles and the D^+ mesons decay to the $\pi^+ K^- \pi^+$ final state with the kaon misidentified as a pion. Data control samples are used to check the agreement with simulation. A control sample representing the $B \to D^{*-} D^0 X$ decays is selected using the decay mode $D^0 \to K^- 3\pi$. The isolation algorithm described in Sec. III A 2 searches for extra kaons around the 3π vertex and thus can be used to select such candidates.

[4]Throughout the paper, $\bar{D}^{**}$ and D_s^{**+} are used to refer to any higher-mass excited charm or charm-strange mesons that decay into the ground-state D^{*-} and D_s^+ meson.

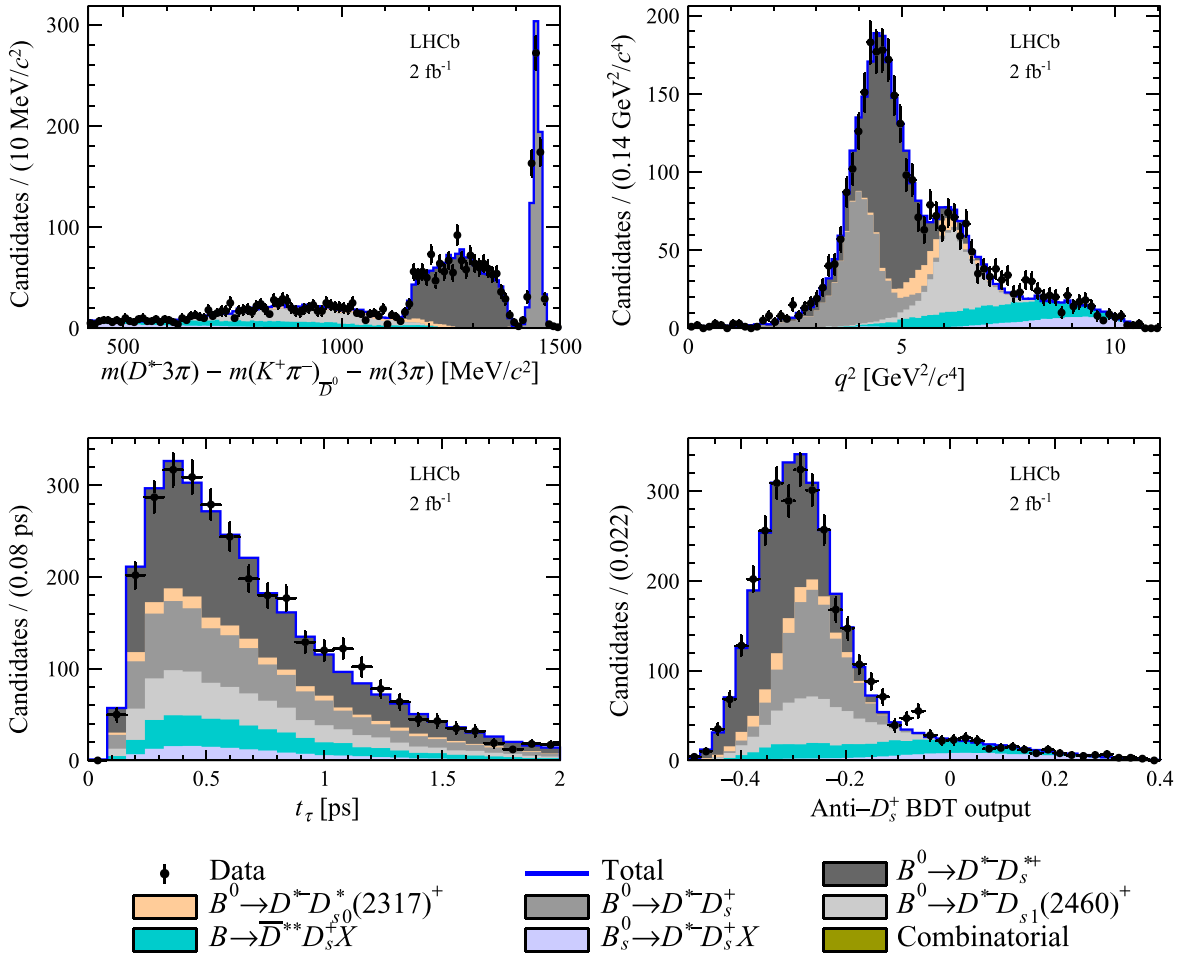

FIG. 2. Distributions of $\Delta M_{D^*D_s}$, q^2, t_τ and anti-D_s^+ BDT output for the $B \to D^{*-}D_s^+(X)$ components. The results of the fit are overlaid.

A $B \to D^{*-}D^+X$ control sample is obtained by reversing the PID requirements on the negatively charged pion to form $D^+ \to \pi^+K^-\pi^+$ decays. In order to retain high statistics, the BDT and B^0 and τ^+ mass requirements are omitted. Other selection criteria remain the same as those for $B^0 \to D^{*-}\tau^+\nu_\tau$ decays.

These control samples are used to check the agreement with simulation for the signal fit variables q^2, t_τ and anti-D_s^+ BDT output. The q^2 distribution shows disagreement between data and simulation in both D^0 and D^+ modes due to the imperfect modeling of inclusive 3π decays. Therefore, the simulation is corrected to match the data distributions. Figure 3 shows the q^2 distributions

TABLE II. Decay fractions for $B \to D^{*-}D_s^+(X)$ decays obtained from data control samples. The fractions are normalized relative to that of the $B^0 \to D^{*-}D_s^{*+}$ decay. $\epsilon_{\text{control}}$ is the efficiency in the control sample.

Parameter	Fit result	$\left(\frac{\epsilon_{\text{sig}}}{\epsilon_{\text{control}}}\right)$	Corrected fraction
$f_{D_s^+}$	0.55 ± 0.03	0.992	0.55 ± 0.03
$f_{D_{s0}^{*+}}$	0.10 ± 0.04	1.077	0.11 ± 0.04
$f_{D_{s1}^+}$	0.37 ± 0.07	1.051	0.39 ± 0.07
$f_{\bar{D}^{**}D_s^+(X)}$	0.28 ± 0.10	1.208	0.34 ± 0.12
$f_{B_s^0 \to D^{*-}D_s^+(X)}$	0.12 ± 0.04	0.904	0.11 ± 0.04

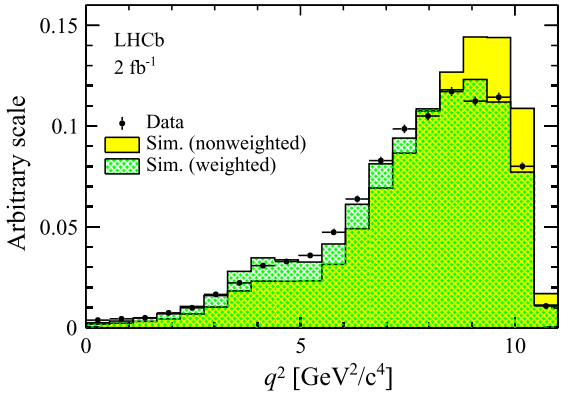

FIG. 3. Simulated q^2 distributions for $B \to D^{*-}D^0(X)$ before and after weighting based on the data control samples.

before and after the corrections in the $B \to D^{*-}D^0(X)$ sample. The agreement is good in the case of the other two fit variables, t_τ and anti-D_s^+ BDT output, and no further correction is necessary.

V. DETERMINATION OF THE SIGNAL AND NORMALIZATION YIELDS

A. $B^0 \to D^{*-}\tau^+\nu_\tau$ yield

The $B^0 \to D^{*-}\tau^+\nu_\tau$ yield is determined from an extended binned maximum-likelihood fit to the distributions of q^2, t_τ and anti-D_s^+ BDT output. The binning scheme comprises eight bins in q^2 and t_τ, and six bins in the BDT output. The chosen binning scheme has maximum sensitivity to the $B^0 \to D^{*-}\tau^+\nu_\tau$ yield while still sufficiently populating the bins. The ranges of q^2, t_τ and BDT distributions are $[0, 11]$ GeV$^2/c^4$, $[0, 2]$ ps and $[-0.2, 0.5]$, respectively. The fit model is built as a three-dimensional template. A summary of the components in the fit model is given in Table III. The fit model assumes that any possible new physics effects on the $B^0 \to D^{*-}\tau^+\nu_\tau$ decays are the same as that in $B \to \bar{D}^{**}\tau^+\nu_\tau$ decays. The templates for the combinatorial components are derived from data in which same-sign combinations of the D^* and τ candidates are selected, whereas the remainder are obtained from simulation.

The fit parameters are itemized below.

(i) $N_{\rm sig}$: The number of $B^0 \to D^{*-}\tau^+\nu_\tau$ events, which is used as input to $\mathcal{K}(D^{*-})$.

(ii) $f_{\tau^+\to 3\pi\bar{\nu}_\tau}$: The fraction of $\tau^+ \to 3\pi\bar{\nu}_\tau$ decays relative to the sum of $\tau^+ \to 3\pi\bar{\nu}_\tau$ and $\tau^+ \to 3\pi\pi^0\bar{\nu}_\tau$ decays. This is estimated and fixed as per the branching fractions and efficiencies of these modes.

TABLE III. List of components in the signal yield extraction fit and their normalization.

Component	Normalization
$B^0 \to D^{*-}\tau^+\nu_\tau$ ($\tau^+ \to 3\pi\bar{\nu}_\tau$)	$N_{\rm sig} \times f_{\tau^+\to 3\pi\bar{\nu}_\tau}$
$B^0 \to D^{*-}\tau^+\nu_\tau$ ($\tau^+ \to 3\pi\pi^0\bar{\nu}_\tau$)	$N_{\rm sig} \times (1 - f_{\tau^+\to 3\pi\bar{\nu}_\tau})$
$B \to \bar{D}^{**}\tau^+\nu_\tau$	$N_{\rm sig} \times f_{\bar{D}^{**}\tau^+\nu}$
$B \to D^{*-}D^0(X)$ same vertex (SV)	$N_{D^0}^{\rm same}$
$B \to D^{*-}D^0(X)$ different vertices (DV)	$N_{D^0}^{\rm same} \times f_{D^0}^{v_1v_2}$
$B \to D^{*-}D^+(X)$	$N_{D_s^+} \times f_{D^+}$
$B^0 \to D^{*-}D_s^+$	$N_{D_s^+} \times f_{D_s^+}/k$
$B^0 \to D^{*-}D_s^{*+}$	$N_{D_s^+} \times 1/k$
$B^0 \to D^{*-}D_{s0}^{*+}$	$N_{D_s^+} \times f_{D_{s0}^{*+}}/k$
$B^0 \to D^{*-}D_{s1}^{+}$	$N_{D_s^+} \times f_{D_{s1}^{+}}/k$
$B \to \bar{D}^{**}D_s^+(X)$	$N_{D_s^+} \times f_{\bar{D}^{**}D_s^+(X)}/k$
$B_s^0 \to D^{*-}D_s^+(X)$	$N_{D_s^+} \times f_{B_s^0\to D^{*-}D_s^+(X)}/k$
$B \to D^{*-}3\pi X$	$N_{B\to D^{*-}3\pi X}$
Combinatorial B	$N_{B_1B_2}$
Combinatorial $\bar{D}^0$	$N_{\rm fake\,\bar{D}^0}$
Combinatorial D^{*-}	$N_{\rm fake\,D^{*-}}$

(iii) $f_{\bar{D}^{**}\tau\nu}$: The amount of $B \to \bar{D}^{**}\tau^+\nu_\tau$ decays relative to $B^0 \to D^{*-}\tau^+\nu_\tau$ decays. This is fixed to the expected value from simulation after correcting for the overestimated branching fractions used to produce them. The correction is done by comparing the theoretical expectations for each $\bar{D}^{**}$ state from the $R(D^{**})$ predictions from Ref. [33] and branching fractions of $B \to \bar{D}^{**}\mu^+\nu_\mu$ [11]. This fraction is determined to be 3.5%, which is significantly lower than that used in Refs. [4,5].

(iv) $N_{D^0}^{\rm same}$: The number of $B \to D^{*-}D^0(X)$ candidates where all pions in the 3π system originate from the D^0 vertex. The yield is estimated from simulation and corrected for data-simulation differences by the ratio of $D^0 \to K^-3\pi$ decays in both samples. This value is fixed in the fit.

(v) $f_{D^0}^{v_1v_2}$: The ratio of the number of $B \to D^{*-}D^0(X)$ decays where at least one of the pions comes from the D^0 vertex and the other pion(s) from a different vertex relative to $N_{D^0}^{\rm same}$.

(vi) f_{D^+}: The ratio of the number of $B \to D^{*-}D^+(X)$ decays to the number of $B \to D^{*-}D_s^+(X)$ decays.

(vii) $N_{D_s^+}$: The yield of $B \to D^{*-}D_s^+(X)$ decays, which have six categories, as described in Sec. IV B. The fraction parameters are Gaussian constrained to the values obtained from the data control sample given in Table II after correcting for efficiency effects.

(viii) $N_{B\to D^{*-}3\pi X}$: The yield of $B \to D^{*-}3\pi X$ events where the three pions come from the B vertex. This value is constrained by using the observed ratio between $B^0 \to D^{*-}3\pi$ exclusive and $B \to D^{*-}3\pi X$ inclusive decays, corrected for data-simulation differences.

(ix) $N_{B_1B_2}$: the yield of combinatorial background events where the D^{*-} meson and the 3π system come from different B decays. It is fixed to the value obtained in the same-sign data sample with $D^{*+}3\pi$ candidates satisfying the criteria of higher mass and nonisolation due to originating from two different b hadrons.

(x) $N_{\rm fake\,\bar{D}^0}$ and $N_{\rm fake\,D^{*-}}$: The combinatorial background yields with a fake $\bar{D}^0$ and D^{*-}, respectively. These are fixed to the values obtained from a fit to $m(K^-\pi^+)$ and $m(D^{*-}) - m(K^-\pi^+)$.

The parameters $N_{\rm sig}$, $N_{D_s^+}$, f_{D^+} and $f_{D^0}^{v_1v_2}$ vary freely in the fit. The fit results are summarized in Table IV and the distributions of the fit variables are shown in Fig. 4. The fit is performed in two iterations: First, the fractions of D^0 are varied freely and the six D_s^+ decay modes are Gaussian constrained, and then a second fit is performed by fixing these to their best fit values. This is the same strategy followed in Refs. [4,5] to determine the statistical uncertainty on the $B^0 \to D^{*-}\tau^+\nu_\tau$ yield. Thus the relative statistical precision on the yield changes from 6.2% to 5.9%. The quadratic difference between the statistical uncertainties in the two iterations is treated as a systematic

TABLE IV. Fit results from the three-dimensional signal-extraction fit to q^2, t_τ and anti-D_s^+ BDT output in the data.

Parameter	Fit result	Constraint
	Free	
$N_{\rm sig}$	2469 ± 154	
$N_{D_s^+}$	20446 ± 509	
f_{D^+}	0.08 ± 0.01	
$f_{D^0}^{v_1 v_2}$	2.10 ± 0.30	
	Constrained	
$N_{B\to D^{*-}3\pi X}$	2279 ± 177	2051 ± 200
$f_{B_s^0\to D^{*-}D_s^+(X)}$	0.13 ± 0.03	0.11 ± 0.04
$f_{D_{s1}^+}$	0.36 ± 0.03	0.40 ± 0.07
$f_{D_s^+}$	0.60 ± 0.02	0.55 ± 0.03
$f_{D_{s0}^{*+}}$	0.06 ± 0.03	0.11 ± 0.04
$f_{\bar{D}^{**}D_s^+(X)}$	0.61 ± 0.06	0.34 ± 0.12
	Fixed	
$N_{B_1B_2}$	46	
$N_{D^0}^{\rm same}$	1051	
$N_{{\rm fake}\bar{D}^0}$	468	
$N_{{\rm fake}D^{*-}}$	714	
$f_{\bar{D}^{**}\tau^+\nu}$	0.035	
$f_{\tau^+\to 3\pi\bar{\nu}_\tau}$	0.780	

uncertainty from the double-charm decay models. The number of signal events is determined to be 2469 ± 154, where the uncertainty is statistical only. The fit quality is excellent with a χ^2 per degree of freedom of 1.0. From studies using pseudoexperiments, the fit is found to be unbiased.

B. $B^0 \to D^{*-}3\pi$ yield

The $B^0 \to D^{*-}3\pi$ yield is estimated from an unbinned maximum-likelihood fit to the $D^{*-}3\pi^\pm$ mass distribution. The signal model consists of a Crystal Ball (CB) function [34] and two Gaussian functions that share a common mean. The CB shape parameters, the width of the wider Gaussian and the relative proportion of the two Gaussian functions are fixed to the values obtained from simulation. The background component is described by an exponential function. The $m(D^{*-}3\pi)$ distribution is shown in Fig. 5 (left) with the fit projection overlaid. The data sample contains $B^0 \to D^{*-}D_s^+(\to 3\pi)$ decays, which must be subtracted from the $B^0 \to D^{*-}3\pi$ yield (Fig. 5, right). A fit to the $m(3\pi)$ distribution in the mass range 1800–2100 MeV/c^2 yields 451 ± 35 decays. After the subtraction, there are 30540 ± 182 $B^0 \to D^{*-}3\pi$ decays. Here, the uncertainties are statistical only.

The $B^0 \to D^{*-}\tau^+\nu_\tau$ and $B^0 \to D^{*-}3\pi$ yields and their efficiencies are used to determine $\mathcal{K}(D^{*-})$, yielding a result

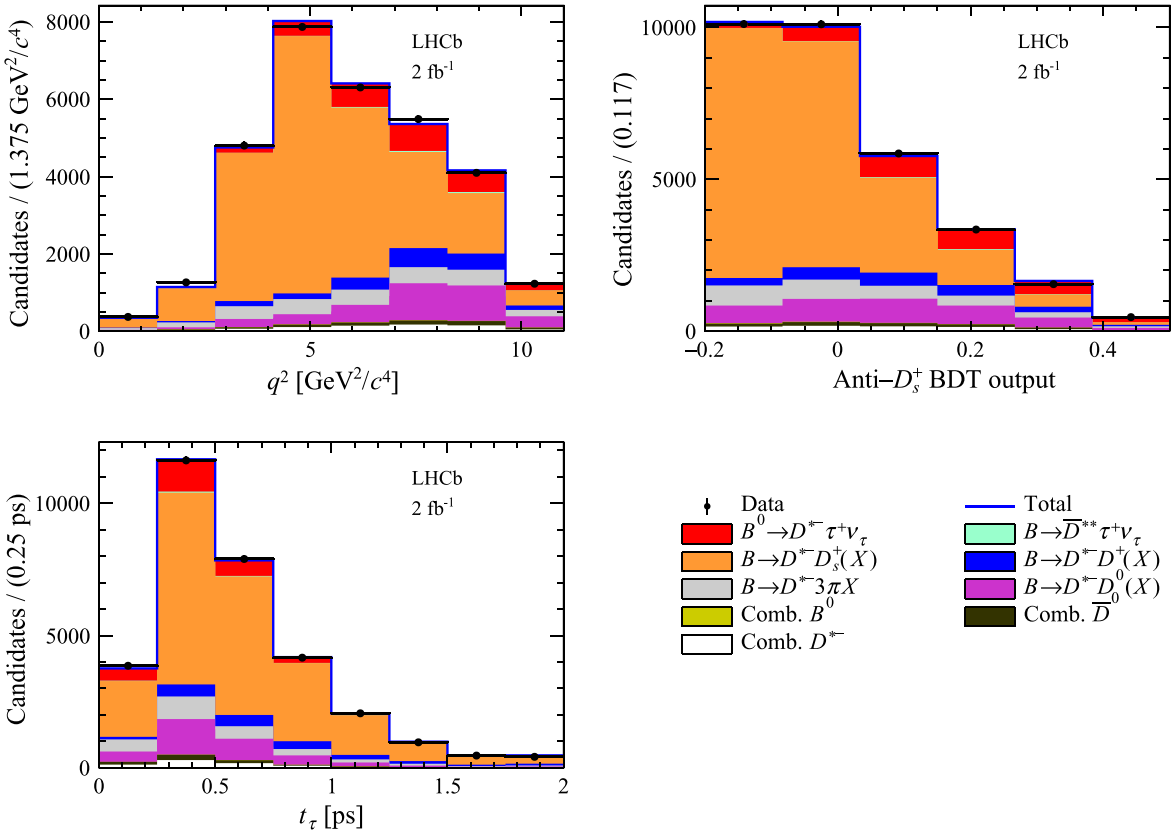

FIG. 4. Distributions of the fit variables in the $B^0 \to D^{*-}\tau^+\nu_\tau$ data sample with the fit result overlaid.

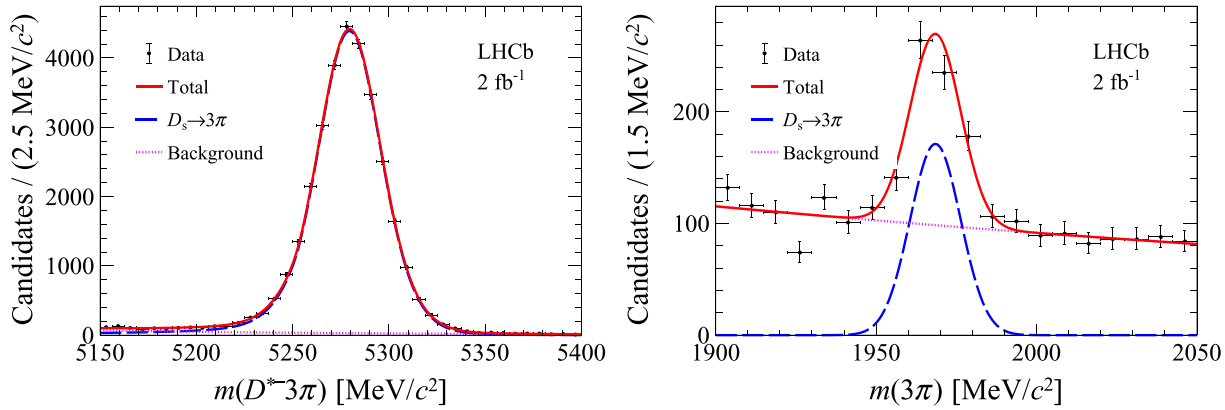

FIG. 5. Invariant-mass distribution of the (left) $D^{*-}3\pi$ and (right) 3π system for $B^0 \to D^{*-}3\pi$ candidates in data with corresponding fit models superimposed.

of $1.70 \pm 0.10^{+0.11}_{-0.10}$, where the uncertainties are statistical and systematic, respectively.

VI. SYSTEMATIC UNCERTAINTIES

Systematic uncertainties on $\mathcal{K}(D^{*-})$ due to the signal and background modeling, selection criteria on the $B^0 \to D^{*-}\tau^+\nu_\tau$ and the $B^0 \to D^{*-}3\pi$ decay modes, empty bins in the fit and limited size of simulation samples are considered.

The simulated $B^0 \to D^{*-}\tau^+\nu_\tau$ decays are weighted with form factors using the Caprini-Lellouch-Neubert parametrization [35] and these are used to produce signal templates for the fit. The systematic uncertainty due to the limited knowledge of the form factors is estimated by changing the baseline to the Boyd-Grinstein-Lebed parametrization [36] and this causes a 1.8% relative change in the signal yield and a 0.9% deviation in the signal efficiency. The fraction between the two signal decay modes $f_{\tau^+\to 3\pi\bar{\nu}_\tau}$ is fixed in the signal fit. The uncertainty on this is estimated by propagating the uncertainties of the branching fractions and efficiencies. A deviation of 0.3% is found from alternate fits with $f_{\tau^+\to 3\pi\bar{\nu}_\tau}$ varied by $\pm 1\sigma$. Other τ^+ decays may contribute to the signal, especially those with three charged hadrons in the final state, e.g., $K^+\,\pi^-\,\pi^+$, $K^+\,K^-\,\pi^+$ or $3\pi\pi^0\pi^0$. They are found to have small contributions in the signal sample after full selection. A detailed study with dedicated simulation samples in Refs. [4,5] found a systematic effect of 1.0% and this is taken as the systematic uncertainty from this source. The fraction of $B \to \bar{D}^{**}\tau^+\nu_\tau$ decays, $f_{\bar{D}^{**}\tau\nu}$, is estimated from simulation after considering theoretical assumptions [33]. This fraction is varied by $\pm 50\%$ and a systematic deviation of $^{+1.8}_{-1.9}\%$ is obtained. The $B^0 \to D^{*-}3\pi$ fit model depends on parameters that are fixed to the values obtained in simulation. These are varied by $\pm 1\sigma$ and the corresponding deviation of 1.0% is assigned as a systematic uncertainty.

The modeling of double-charm, prompt and combinatorial backgrounds contribute to the systematic uncertainty on $\mathcal{K}(D^{*-})$. The D_s^+ decays in simulation are corrected by the weights obtained in the fit to the $D_s^+ \to 3\pi X$ control sample. These weights are varied by their uncertainties after accounting for correlations and alternate signal-extraction fits are performed with the new D_s^+ templates. This results in a 1.0% systematic deviation in $\mathcal{K}(D^{*-})$. The fixed fraction of $D_s^+ \to Ra_1$ in the fit to the $D_s^+ \to 3\pi X$ control sample is varied by 30% and this contributes to a 1.5% systematic deviation. This variation corresponds to a change of 1 in the χ^2 of the signal-extraction fit.

The variables in the signal-extraction fit, q^2, t_τ and the anti-D_s^+ BDT output, can have a non-negligible correlation with some important kinematic variables like $m(D^{*-}3\pi)$, $m(3\pi)$, $\min[m(\pi^+\pi^-)]$ and $\max[m(\pi^+\pi^-)]$ that are used in background studies. The background template shapes that are derived from simulation are varied with weights that are functions of these kinematic variables. The signal-extraction fit is repeated with the alternate templates for the different background categories to estimate the systematic effect on the results. The variations in the D_s^+, D^0, D^+ and prompt template shapes result in 0.3%, 1.2%, $^{+2.2}_{-0.8}\%$ and 1.2% deviations, respectively, to $\mathcal{K}(D^{*-})$. The effect of fixing the D^+ and D^0 fractions (f_{D^+} and $f_{D^0}^{v_1 v_2}$) as well as combinatorial yields are estimated by varying the fixed values by their uncertainties.

The efficiencies of particle identification requirements are estimated using calibration samples. These samples are used to parametrize the efficiency in bins of the kinematic variables of a given track such as p, p_{T} and hits in the tracking system. The choice of the binning scheme for this parametrization contributes a 0.5% systematic uncertainty. The effect of the finite size of the calibration sample is negligible. The systematic effects of the correction weights applied to the simulation are obtained either by varying the correction factor or removing the correction altogether.

Changes in kinematic weighting, 3π vertex error correction and 3π model correction in $B^0 \to D^{*-}3\pi$ decays result in 0.7%, 0.9% and 1.0% systematic deviations, respectively, on $\mathcal{K}(D^{*-})$. The difference in data and simulation at the preselection level affects the efficiency determination, contributing 2.0% to the systematic uncertainty. The statistical uncertainty on the $B^0 \to D^{*-}\tau^+\nu_\tau$ and $B^0 \to D^{*-}3\pi$ efficiencies due to the limited size of the simulation sample also contribute to the systematic uncertainty.

The three-dimensional templates used in the fit include empty bins. The systematic deviation due to these empty bins is estimated by building a three-dimensional density function using kernel density estimators. These are built for all the components and then transformed into a histogram template and the fit is repeated with the new templates. This contributes to a 1.3% relative systematic deviation.

The template PDFs used in the signal fit are mostly derived from simulation. Therefore, the size of these simulation samples has a major impact on the results. Alternative templates obtained after resampling the default templates via a bootstrap procedure are used to repeat the fit 1000 times and the resulting deviation of 2.0% is taken as the systematic uncertainty from this source. The large simulation samples produced using the ReDecay [31] technique helped in reducing this systematic uncertainty to half the value obtained in Refs. [4,5]. A summary of all the systematic uncertainties on $\mathcal{K}(D^{*-})$ is given in Table V. The total systematic uncertainty is obtained by adding the individual contributions in quadrature.

TABLE V. Summary of relative systematic uncertainties on the ratio $\mathcal{K}(D^{*-})$.

Source	Systematic uncertainty (%)
Signal decay template shape	1.8
Signal decay efficiency	0.9
Fractions of signal τ^+ decays	0.3
Possible contributions from other τ^+ decays	1.0
Fixing the $\bar{D}^{**}\tau^+\nu_\tau$ and $D_s^{**+}\tau^+\nu_\tau$ fractions	$^{+1.8}_{-1.9}$
Normalization mode PDF choice	1.0
Knowledge of the $D_s^+ \to 3\pi X$ decay model	1.0
Specifically the $D_s^+ \to a_1 X$ fraction	1.5
$B \to D^{*-}D_s^+(X)$ template shapes	0.3
$B \to D^{*-}D^0(X)$ template shapes	1.2
$B \to D^{*-}D^+(X)$ template shapes	$^{+2.2}_{-0.8}$
Fixing $B \to D^{*-}D_s^+(X)$ background model parameters	1.1
Fixing $B \to D^{*-}D^0(X)$ background model parameters	1.5
$B \to D^{*-}3\pi X$ template shapes	1.2
Combinatorial background normalization	$^{+0.5}_{-0.6}$
PID efficiency	0.5
Kinematic reweighting	0.7
Vertex error correction	0.9
Normalization mode efficiency [modeling of $m(3\pi)$]	1.0
Preselection efficiency	2.0
Signal efficiency (size of simulation sample)	1.1
Normalization efficiency (size of simulation sample)	1.1
Empty bins in templates	1.3
PDF shapes uncertainty (size of simulation sample)	2.0
Total systematic uncertainty	$^{+6.2}_{-5.9}$
Total statistical uncertainty	5.9

VII. CONCLUSION

In conclusion, using pp collision data collected in 2015 and 2016 by the LHCb experiment and corresponding to an integrated luminosity of 2 fb^{-1}, the ratio of the branching fractions of $B^0 \to D^{*-}\tau^+\nu_\tau$ and $B^0 \to D^{*-}3\pi$ decays is measured as

$$\mathcal{K}(D^{*-}) = 1.70 \pm 0.10(\text{stat})^{+0.11}_{-0.10}(\text{syst}).$$

The result is in good agreement with the previous LHCb measurement [4,5]. The improved analysis procedure results in an increase in signal efficiency and a decrease of the relative systematic uncertainty from 9% to 6%. Using the most recent branching fraction measurements $\mathcal{B}(B^0 \to D^{*-}3\pi) = (7.21 \pm 0.29) \times 10^{-3}$ and $\mathcal{B}(B^0 \to D^{*-}\mu^+\nu_\mu) = (4.97 \pm 0.12)\%$ [11], the branching fraction

$$\mathcal{B}(B^0 \to D^{*-}\tau^+\nu_\tau) = (1.23 \pm 0.07(\text{stat})^{+0.08}_{-0.07}(\text{syst}) \pm 0.05(\text{ext})) \times 10^{-2},$$

and the ratio of branching fractions of $B^0 \to D^{*-}\tau^+\nu_\tau$ and $B^0 \to D^{*-}\mu^+\nu_\mu$,

$$\mathcal{R}(D^{*-}) = 0.247 \pm 0.015(\text{stat}) \pm 0.015(\text{syst}) \pm 0.012(\text{ext})$$

are obtained, where the third uncertainties are due to the uncertainties on the external branching fractions. This result is compatible with the present world average and with the SM expectation (0.254 ± 0.005) [7]. When combined with the previous results [4,5], the values of $\mathcal{K}(D^{*-})$ and $\mathcal{R}(D^{*-})$ are

$$\mathcal{K}(D^{*-})_{\text{comb}} = 1.77 \pm 0.08(\text{stat}) \pm 0.10(\text{syst}) \quad \text{and}$$
$$\mathcal{R}(D^{*-})_{\text{comb}} = 0.257 \pm 0.012(\text{stat}) \pm 0.014(\text{syst}) \pm 0.012(\text{ext}).$$

The combined $\mathcal{R}(D^{*-})$ is obtained from the $\mathcal{K}(D^{*-})$ combination and the branching fractions of the normalization channels. This combination leads to one of the most precise measurements of $\mathcal{R}(D^*)$ to date.

ACKNOWLEDGMENTS

We express our gratitude to our colleagues in the CERN accelerator departments for the excellent performance of the LHC. We thank the technical and administrative staff at the LHCb institutes. We acknowledge support from CERN and from the national agencies: CAPES, CNPq, FAPERJ and FINEP (Brazil); MOST and NSFC (China); CNRS/IN2P3 (France); BMBF, DFG and MPG (Germany); INFN (Italy); NWO (Netherlands); MNiSW and NCN (Poland); MEN/IFA (Romania); MICINN (Spain); SNSF and SER (Switzerland); NASU (Ukraine); STFC (United Kingdom); DOE NP and NSF (USA). We acknowledge the computing resources that are provided by CERN, IN2P3 (France), KIT and DESY (Germany), INFN (Italy), SURF (Netherlands), PIC (Spain), GridPP (United Kingdom), CSCS (Switzerland), IFIN-HH (Romania), CBPF (Brazil), Polish WLCG (Poland) and NERSC (USA). We are indebted to the communities behind the multiple open-source software packages on which we depend. Individual groups or members have received support from ARC and ARDC (Australia); Minciencias (Colombia); AvH Foundation (Germany); EPLANET, Marie Skłodowska-Curie Actions and ERC (European Union); A*MIDEX, ANR, IPhU and Labex P2IO, and Région Auvergne-Rhône-Alpes (France); Key Research Program of Frontier Sciences of CAS, CAS PIFI, CAS CCEPP, Fundamental Research Funds for the Central Universities, and Science and Technology Program of Guangzhou (China); GVA, XuntaGal, GENCAT and Prog. Atracción Talento, CM (Spain); SRC (Sweden); the Leverhulme Trust, the Royal Society and UKRI (United Kingdom).

[1] J. P. Lees *et al.* (*BABAR* Collaboration), Evidence for an Excess of $\bar{B} \to D^{(*)}\tau^-\bar{\nu}_\tau$ Decays, Phys. Rev. Lett. **109**, 101802 (2012).

[2] M. Huschle *et al.* (Belle Collaboration), Measurement of the branching ratio of $\bar{B} \to D^{(*)}\tau^-\bar{\nu}_\tau$ relative to $\bar{B} \to D^{(*)}\ell^-\bar{\nu}_\ell$ decays with hadronic tagging at Belle, Phys. Rev. D **92**, 072014 (2015).

[3] S. Hirose *et al.* (Belle Collaboration), Measurement of the τ lepton polarization and $R(D^*)$ in the decay $\bar{B} \to D^*\tau^-\bar{\nu}_\tau$ with one-prong hadronic τ decays at Belle, Phys. Rev. D **97**, 012004 (2018).

[4] R. Aaij *et al.* (LHCb Collaboration), Measurement of the Ratio of the $\mathcal{B}(B^0 \to D^{*-}\tau^+\nu_\tau)$ and $\mathcal{B}(B^0 \to D^{*-}\mu^+\nu_\mu)$ Branching Fractions Using Three-Prong τ-Lepton Decays, Phys. Rev. Lett. **120**, 171802 (2018).

[5] R. Aaij *et al.* (LHCb Collaboration), Test of lepton flavor universality by the measurement of the $B^0 \to D^{*-}\tau^+\nu_\tau$ branching fraction using three-prong τ decays, Phys. Rev. D **97**, 072013 (2018).

[6] R. Aaij *et al.* (LHCb Collaboration), Measurement of the ratio of branching fractions $\mathcal{R}(D^*)$ and $\mathcal{R}(D^0)$, arXiv:2302.02886.

[7] Y. Amhis *et al.* (HFLAV Collaboration), Averages of b-hadron, c-hadron, and τ-lepton properties as of 2021, Phys. Rev. D **107**, 052008 (2023).

[8] S. Fajfer, J. F. Kamenik, and I. Nisandzic, On the $B \to D^*\tau\bar{\nu}_\tau$ sensitivity to new physics, Phys. Rev. D **85**, 094025 (2012).

[9] S. Fajfer and N. Košnik, Vector leptoquark resolution of R_K and $R_{D^{(*)}}$ puzzles, Phys. Lett. B **755**, 270 (2016).

[10] A. Crivellin, D. Müller, and T. Ota, Simultaneous explanation of $R(D^{(*)})$ and $b \to s\mu^+\mu^-$: The last scalar leptoquarks standing, J. High Energy Phys. 09 (2017) 040.

[11] R. L. Workman *et al.* (Particle Data Group), Review of particle physics, Prog. Theor. Exp. Phys. **2022**, 083C01 (2022).

[12] A. A. Alves, Jr. *et al.* (LHCb Collaboration), The LHCb detector at the LHC, J. Instrum. **3**, S08005 (2008).

[13] LHCb Collaboration, LHCb detector performance, Int. J. Mod. Phys. A **30**, 1530022 (2015).

[14] R. Aaij *et al.*, Performance of the LHCb vertex locator, J. Instrum. **9**, P09007 (2014).

[15] R. Arink *et al.*, Performance of the LHCb outer tracker, J. Instrum. **9**, P01002 (2014).

[16] P. d'Argent *et al.*, Improved performance of the LHCb outer tracker in LHC Run 2, J. Instrum. **12**, P11016 (2017).

[17] M. Adinolfi *et al.*, Performance of the LHCb RICH detector at the LHC, Eur. Phys. J. C **73**, 2431 (2013).

[18] A. A. Alves, Jr. *et al.*, Performance of the LHCb muon system, J. Instrum. **8**, P02022 (2013).

[19] R. Aaij *et al.*, The LHCb trigger and its performance in 2011, J. Instrum. **8**, P04022 (2013).

[20] V. V. Gligorov and M. Williams, Efficient, reliable and fast high-level triggering using a bonsai boosted decision tree, J. Instrum. **8**, P02013 (2013).

[21] T. Likhomanenko, P. Ilten, E. Khairullin, A. Rogozhnikov, A. Ustyuzhanin, and M. Williams, LHCb topological trigger reoptimization, J. Phys. Conf. Ser. **664**, 082025 (2015).

[22] T. Sjöstrand, S. Mrenna, and P. Skands, A brief introduction to PYTHIA 8.1, Comput. Phys. Commun. **178**, 852 (2008); PYTHIA 6.4 physics and manual, J. High Energy Phys. 05 (2006) 026.

[23] I. Belyaev *et al.*, Handling of the generation of primary events in Gauss, the LHCb simulation framework, J. Phys. Conf. Ser. **331**, 032047 (2011).

[24] D. J. Lange, The EvtGen particle decay simulation package, Nucl. Instrum. Methods Phys. Res., Sect. A **462**, 152 (2001).

[25] N. Davidson, T. Przedzinski, and Z. Was, PHOTOS interface in C++: Technical and physics documentation, Comput. Phys. Commun. **199**, 86 (2016).

[26] I. M. Nugent, T. Przedziński, P. Roig, O. Shekhovtsova, and Z. Wąs, Resonance chiral Lagrangian currents and experimental data for $\tau^- \to \pi^-\pi^-\pi^+\nu_\tau$, Phys. Rev. D **88**, 093012 (2013).
[27] N. Davidson, G. Nanava, T. Przedziński, E. Richter-Wąs, and Z. Wąs, Universal interface of TAUOLA: Technical and physics documentation, Comput. Phys. Commun. **183**, 821 (2012).
[28] I. M. Nugent, Invariant mass spectra of $\tau^- \to h^-h^-h^+\nu_\tau$ decays, Nucl. Phys. B, Proc. Suppl. **253–255**, 38 (2014).
[29] J. Allison *et al.* (Geant4 Collaboration), Geant4 developments and applications, IEEE Trans. Nucl. Sci. **53**, 270 (2006); S. Agostinelli *et al.* (Geant4 Collaboration), Geant4: A simulation toolkit, Nucl. Instrum. Methods Phys. Res., Sect. A **506**, 250 (2003).
[30] M. Clemencic, G. Corti, S. Easo, C. R. Jones, S. Miglioranzi, M. Pappagallo, and P. Robbe, The LHCb simulation application, Gauss: Design, evolution and experience, J. Phys. Conf. Ser. **331**, 032023 (2011).
[31] D. Müller, M. Clemencic, G. Corti, and M. Gersabeck, ReDecay: A novel approach to speed up the simulation at LHCb, Eur. Phys. J. C **78**, 1009 (2018).
[32] R. Aaij *et al.* (LHCb Collaboration), A precise measurement of the B^0 meson oscillation frequency, Eur. Phys. J. C **76**, 412 (2016).
[33] F. U. Bernlochner, M. F. Sevilla, D. J. Robinson, and G. Wormser, Semitauonic b-hadron decays: A lepton flavor universality laboratory, Rev. Mod. Phys. **94**, 015003 (2022).
[34] T. Skwarnicki, A study of the radiative CASCADE transitions between the Upsilon-prime and Upsilon resonances, Ph.D. thesis, Institute of Nuclear Physics, Krakow, 1986.
[35] I. Caprini, L. Lellouch, and M. Neubert, Dispersive bounds on the shape of $\bar{B} \to D^{(*)}\ell\bar{\nu}$ form factors, Nucl. Phys. **B530**, 153 (1998).
[36] C. G. Boyd, B. Grinstein, and R. F. Lebed, Model-independent determinations of $\bar{B} \to D\ell\bar{\nu}$, $D^*\ell\bar{\nu}$ form factors, Nucl. Phys. **B461**, 493 (1996).

R. Aaij,[32] A. S. W. Abdelmotteleb,[51] C. Abellan Beteta,[45] F. Abudinén,[51] T. Ackernley,[55] B. Adeva,[41] M. Adinolfi,[49] P. Adlarson,[77] H. Afsharnia,[9] C. Agapopoulou,[13] C. A. Aidala,[78] Z. Ajaltouni,[9] S. Akar,[60] K. Akiba,[32] P. Albicocco,[23] J. Albrecht,[15] F. Alessio,[43] M. Alexander,[54] A. Alfonso Albero,[40] Z. Aliouche,[57] P. Alvarez Cartelle,[50] R. Amalric,[13] S. Amato,[2] J. L. Amey,[49] Y. Amhis,[11,43] L. An,[43] L. Anderlini,[22] M. Andersson,[45] A. Andreianov,[38] M. Andreotti,[21] D. Andreou,[63] D. Ao,[6] F. Archilli,[31,b] A. Artamonov,[38] M. Artuso,[63] E. Aslanides,[10] M. Atzeni,[45] B. Audurier,[12] I. B Bachiller Perea,[8] S. Bachmann,[17] M. Bachmayer,[44] J. J. Back,[51] A. Bailly-reyre,[13] P. Baladron Rodriguez,[41] V. Balagura,[12] W. Baldini,[21,43] J. Baptista de Souza Leite,[1] M. Barbetti,[22,c] R. J. Barlow,[57] S. Barsuk,[11] W. Barter,[53] M. Bartolini,[50] F. Baryshnikov,[38] J. M. Basels,[14] G. Bassi,[29,d] B. Batsukh,[4] A. Battig,[15] A. Bay,[44] A. Beck,[51] M. Becker,[15] F. Bedeschi,[29] I. B. Bediaga,[1] A. Beiter,[63] S. Belin,[41] V. Bellee,[45] K. Belous,[38] I. Belov,[38] I. Belyaev,[38] G. Benane,[10] G. Bencivenni,[23] E. Ben-Haim,[13] A. Berezhnoy,[38] R. Bernet,[45] S. Bernet Andres,[39] D. Berninghoff,[17] H. C. Bernstein,[63] C. Bertella,[57] A. Bertolin,[28] C. Betancourt,[45] F. Betti,[43] Ia. Bezshyiko,[45] J. Bhom,[35] L. Bian,[69] M. S. Bieker,[15] N. V. Biesuz,[21] P. Billoir,[13] A. Biolchini,[32] M. Birch,[56] F. C. R. Bishop,[50] A. Bitadze,[57] A. Bizzeti, M. P. Blago,[50] T. Blake,[51] F. Blanc,[44] J. E. Blank,[15] S. Blusk,[63] D. Bobulska,[54] V. B Bocharnikov,[38] J. A. Boelhauve,[15] O. Boente Garcia,[12] T. Boettcher,[60] A. Boldyrev,[38] C. S. Bolognani,[75] R. Bolzonella,[21,e] N. Bondar,[38,43] F. Borgato,[28] S. Borghi,[57] M. Borsato,[17] J. T. Borsuk,[35] S. A. Bouchiba,[44] T. J. V. Bowcock,[55] A. Boyer,[43] C. Bozzi,[21] M. J. Bradley,[56] S. Braun,[61] A. Brea Rodriguez,[41] N. Breer,[15] J. Brodzicka,[35] A. Brossa Gonzalo,[41] J. Brown,[55] D. Brundu,[27] A. Buonaura,[45] L. Buonincontri,[28] A. T. Burke,[57] C. Burr,[43] A. Bursche,[67] A. Butkevich,[38] J. S. Butter,[32] J. Buytaert,[43] W. Byczynski,[43] S. Cadeddu,[27] H. Cai,[69] R. Calabrese,[21,e] L. Calefice,[15] S. Cali,[23] M. Calvi,[26,f] M. Calvo Gomez,[39] P. Campana,[23] D. H. Campora Perez,[75] A. F. Campoverde Quezada,[6] S. Capelli,[26,f] L. Capriotti,[20] A. Carbone,[20,g] R. Cardinale,[24,h] A. Cardini,[27] P. Carniti,[26,f] L. Carus,[14] A. Casais Vidal,[41] R. Caspary,[17] G. Casse,[55] M. Cattaneo,[43] G. Cavallero,[21] V. Cavallini,[21,e] S. Celani,[44] J. Cerasoli,[10] D. Cervenkov,[58] A. J. Chadwick,[55] I. C Chahrour,[78] M. G. Chapman,[49] M. Charles,[13] Ph. Charpentier,[43] C. A. Chavez Barajas,[55] M. Chefdeville,[8] C. Chen,[10] S. Chen,[4] A. Chernov,[35] S. Chernyshenko,[47] V. Chobanova,[41] S. Cholak,[44] M. Chrzaszcz,[35] A. Chubykin,[38] V. Chulikov,[38] P. Ciambrone,[23] M. F. Cicala,[51] X. Cid Vidal,[41] G. Ciezarek,[43] P. Cifra,[43] G. Ciullo,[21,e] P. E. L. Clarke,[53] M. Clemencic,[43] H. V. Cliff,[50] J. Closier,[43] J. L. Cobbledick,[57] V. Coco,[43] J. Cogan,[10] E. Cogneras,[9] L. Cojocariu,[37] P. Collins,[43] T. Colombo,[43] L. Congedo,[19] A. Contu,[27] N. Cooke,[48] I. Corredoira,[41] G. Corti,[43] B. Couturier,[43] D. C. Craik,[45] M. Cruz Torres,[1,i] R. Currie,[53] C. L. Da Silva,[62] S. Dadabaev,[38] L. Dai,[66] X. Dai,[5] E. Dall'Occo,[15] J. Dalseno,[41] C. D'Ambrosio,[43] J. Daniel,[9] A. Danilina,[38]

P. d'Argent,[19] J. E. Davies,[57] A. Davis,[57] O. De Aguiar Francisco,[57] J. de Boer,[43] K. De Bruyn,[74] S. De Capua,[57] M. De Cian,[44] U. De Freitas Carneiro Da Graca,[1] E. De Lucia,[23] J. M. De Miranda,[1] L. De Paula,[2] M. De Serio,[19,j] D. De Simone,[45] P. De Simone,[23] F. De Vellis,[15] J. A. de Vries,[75] C. T. Dean,[62] F. Debernardis,[19,j] D. Decamp,[8] V. Dedu,[10] L. Del Buono,[13] B. Delaney,[59] H.-P. Dembinski,[15] V. Denysenko,[45] O. Deschamps,[9] F. Dettori,[27,k] B. Dey,[72] P. Di Nezza,[23] I. Diachkov,[38] S. Didenko,[38] L. Dieste Maronas,[41] S. Ding,[63] V. Dobishuk,[47] A. Dolmatov,[38] C. Dong,[3] A. M. Donohoe,[18] F. Dordei,[27] A. C. dos Reis,[1] L. Douglas,[54] A. G. Downes,[8] P. Duda,[76] M. W. Dudek,[35] L. Dufour,[43] V. Duk,[73] P. Durante,[43] M. M. Duras,[76] J. M. Durham,[62] D. Dutta,[57] A. Dziurda,[35] A. Dzyuba,[38] S. Easo,[52] U. Egede,[64] V. Egorychev,[38] C. Eirea Orro,[41] S. Eisenhardt,[53] E. Ejopu,[57] S. Ek-In,[44] L. Eklund,[77] M. E Elashri,[60] J. Ellbracht,[15] S. Ely,[56] A. Ene,[37] E. Epple,[60] S. Escher,[14] J. Eschle,[45] S. Esen,[45] T. Evans,[57] F. Fabiano,[27,k] L. N. Falcao,[1] Y. Fan,[6] B. Fang,[11,69] L. Fantini,[73,l] M. Faria,[44] S. Farry,[55] D. Fazzini,[26,f] L. F Felkowski,[76] M. Feo,[43] M. Fernandez Gomez,[41] A. D. Fernez,[61] F. Ferrari,[20] L. Ferreira Lopes,[44] F. Ferreira Rodrigues,[2] S. Ferreres Sole,[32] M. Ferrillo,[45] M. Ferro-Luzzi,[43] S. Filippov,[38] R. A. Fini,[19] M. Fiorini,[21,e] M. Firlej,[34] K. M. Fischer,[58] D. S. Fitzgerald,[78] C. Fitzpatrick,[57] T. Fiutowski,[34] F. Fleuret,[12] M. Fontana,[20] F. Fontanelli,[24,h] R. Forty,[43] D. Foulds-Holt,[50] V. Franco Lima,[55] M. Franco Sevilla,[61] M. Frank,[43] E. Franzoso,[21,e] G. Frau,[17] C. Frei,[43] D. A. Friday,[57] L. F Frontini,[25,m] J. Fu,[6] Q. Fuehring,[15] T. Fulghesu,[13] E. Gabriel,[32] G. Galati,[19,j] M. D. Galati,[32] A. Gallas Torreira,[41] D. Galli,[20,g] S. Gambetta,[53,43] M. Gandelman,[2] P. Gandini,[25] H. G Gao,[6] R. Gao,[58] Y. Gao,[7] Y. Gao,[5] M. Garau,[27,k] L. M. Garcia Martin,[51] P. Garcia Moreno,[40] J. García Pardiñas,[43] B. Garcia Plana,[41] F. A. Garcia Rosales,[12] L. Garrido,[40] C. Gaspar,[43] R. E. Geertsema,[32] D. Gerick,[17] L. L. Gerken,[15] E. Gersabeck,[57] M. Gersabeck,[57] T. Gershon,[51] L. Giambastiani,[28] V. Gibson,[50] H. K. Giemza,[36] A. L. Gilman,[58] M. Giovannetti,[23] A. Gioventù,[41] P. Gironella Gironell,[40] C. Giugliano,[21,e] M. A. Giza,[35] K. Gizdov,[53] E. L. Gkougkousis,[43] V. V. Gligorov,[13,43] C. Göbel,[65] E. Golobardes,[39] D. Golubkov,[38] A. Golutvin,[56,38] A. Gomes,[1,n] S. Gomez Fernandez,[40] F. Goncalves Abrantes,[58] M. Goncerz,[35] G. Gong,[3] I. V. Gorelov,[38] C. Gotti,[26] J. P. Grabowski,[71] T. Grammatico,[13] L. A. Granado Cardoso,[43] E. Graugés,[40] E. Graverini,[44] G. Graziani, A. T. Grecu,[37] L. M. Greeven,[32] N. A. Grieser,[60] L. Grillo,[54] S. Gromov,[38] B. R. Gruberg Cazon,[58] C. Gu,[3] M. Guarise,[21,e] M. Guittiere,[11] P. A. Günther,[17] E. Gushchin,[38] A. Guth,[14] Y. Guz,[5,38,43] T. Gys,[43] T. Hadavizadeh,[64] C. Hadjivasiliou,[61] G. Haefeli,[44] C. Haen,[43] J. Haimberger,[43] S. C. Haines,[50] T. Halewood-leagas,[55] M. M. Halvorsen,[43] P. M. Hamilton,[61] J. Hammerich,[55] Q. Han,[7] X. Han,[17] S. Hansmann-Menzemer,[17] L. Hao,[6] N. Harnew,[58] T. Harrison,[55] C. Hasse,[43] M. Hatch,[43] J. He,[6,o] K. Heijhoff,[32] F. H Hemmer,[43] C. Henderson,[60] R. D. L. Henderson,[64,51] A. M. Hennequin,[59] K. Hennessy,[55] L. Henry,[43] J. H Herd,[56] J. Heuel,[14] A. Hicheur,[2] D. Hill,[44] M. Hilton,[57] S. E. Hollitt,[15] J. Horswill,[57] R. Hou,[7] Y. Hou,[8] J. Hu,[17] J. Hu,[67] W. Hu,[5] X. Hu,[3] W. Huang,[6] X. Huang,[69] W. Hulsbergen,[32] R. J. Hunter,[51] M. Hushchyn,[38] D. Hutchcroft,[55] P. Ibis,[15] M. Idzik,[34] D. Ilin,[38] P. Ilten,[60] A. Inglessi,[38] A. Iniukhin,[38] A. Ishteev,[38] K. Ivshin,[38] R. Jacobsson,[43] H. Jage,[14] S. J. Jaimes Elles,[42] S. Jakobsen,[43] E. Jans,[32] B. K. Jashal,[42] A. Jawahery,[61] V. Jevtic,[15] E. Jiang,[61] X. Jiang,[4,6] Y. Jiang,[6] M. John,[58] D. Johnson,[59] C. R. Jones,[50] T. P. Jones,[51] S. J Joshi,[36] B. Jost,[43] N. Jurik,[43] I. Juszczak,[35] S. Kandybei,[46] Y. Kang,[3] M. Karacson,[43] D. Karpenkov,[38] M. Karpov,[38] J. W. Kautz,[60] F. Keizer,[43] D. M. Keller,[63] M. Kenzie,[51] T. Ketel,[32] B. Khanji,[63] A. Kharisova,[38] S. Kholodenko,[38] G. Khreich,[11] T. Kirn,[14] V. S. Kirsebom,[44] O. Kitouni,[59] S. Klaver,[33] N. Kleijne,[29,d] K. Klimaszewski,[36] M. R. Kmiec,[36] S. Koliiev,[47] L. Kolk,[15] A. Kondybayeva,[38] A. Konoplyannikov,[38] P. Kopciewicz,[34] R. Kopecna,[17] P. Koppenburg,[32] M. Korolev,[38] I. Kostiuk,[32] O. Kot,[47] S. Kotriakhova, A. Kozachuk,[38] P. Kravchenko,[38] L. Kravchuk,[38] M. Kreps,[51] S. Kretzschmar,[14] P. Krokovny,[38] W. Krupa,[34] W. Krzemien,[36] J. Kubat,[17] S. Kubis,[76] W. Kucewicz,[35] M. Kucharczyk,[35] V. Kudryavtsev,[38] E. K Kulikova,[38] A. Kupsc,[77] D. Lacarrere,[43] G. Lafferty,[57] A. Lai,[27] A. Lampis,[27,k] D. Lancierini,[45] C. Landesa Gomez,[41] J. J. Lane,[57] R. Lane,[49] C. Langenbruch,[14] J. Langer,[15] O. Lantwin,[38] T. Latham,[51] F. Lazzari,[29,p] C. Lazzeroni,[48] R. Le Gac,[10] S. H. Lee,[78] R. Lefèvre,[9] A. Leflat,[38] S. Legotin,[38] P. Lenisa,[21,e] O. Leroy,[10] T. Lesiak,[35] B. Leverington,[17] A. Li,[3] H. Li,[67] K. Li,[7] P. Li,[43] P.-R. Li,[68] S. Li,[7] T. Li,[4] T. Li,[67] Y. Li,[4] Z. Li,[63] X. Liang,[63] C. Lin,[6] T. Lin,[52] R. Lindner,[43] V. Lisovskyi,[15] R. Litvinov,[27,k] G. Liu,[67] H. Liu,[6] K. Liu,[68] Q. Liu,[6] S. Liu,[4,6] A. Lobo Salvia,[40] A. Loi,[27] R. Lollini,[73] J. Lomba Castro,[41] I. Longstaff,[54] J. H. Lopes,[2] A. Lopez Huertas,[40] S. López Soliño,[41]

G. H. Lovell,[50] Y. Lu,[4,q] C. Lucarelli,[22,c] D. Lucchesi,[28,r] S. Luchuk,[38] M. Lucio Martinez,[75] V. Lukashenko,[32,47] Y. Luo,[3] A. Lupato,[57] E. Luppi,[21,e] A. Lusiani,[29,d] K. Lynch,[18] X.-R. Lyu,[6] R. Ma,[6] S. Maccolini,[15] F. Machefert,[11] F. Maciuc,[37] I. Mackay,[58] V. Macko,[44] L. R. Madhan Mohan,[50] A. Maevskiy,[38] D. Maisuzenko,[38] M. W. Majewski,[34] J. J. Malczewski,[35] S. Malde,[58] B. Malecki,[35,43] A. Malinin,[38] T. Maltsev,[38] G. Manca,[27,k] G. Mancinelli,[10] C. Mancuso,[11,25,m] R. Manera Escalero,[40] D. Manuzzi,[20] C. A. Manzari,[45] D. Marangotto,[25,m] J. M. Maratas,[9,s] J. F. Marchand,[8] U. Marconi,[20] S. Mariani,[43] C. Marin Benito,[40] J. Marks,[17] A. M. Marshall,[49] P. J. Marshall,[55] G. Martelli,[73,l] G. Martellotti,[30] L. Martinazzoli,[43,f] M. Martinelli,[26,f] D. Martinez Santos,[41] F. Martinez Vidal,[42] A. Massafferri,[1] M. Materok,[14] R. Matev,[43] A. Mathad,[45] V. Matiunin,[38] C. Matteuzzi,[26] K. R. Mattioli,[12] A. Mauri,[56] E. Maurice,[12] J. Mauricio,[40] M. Mazurek,[43] M. McCann,[56] L. Mcconnell,[18] T. H. McGrath,[57] N. T. McHugh,[54] A. McNab,[57] R. McNulty,[18] B. Meadows,[60] G. Meier,[15] D. Melnychuk,[36] S. Meloni,[26,f] M. Merk,[32,75] A. Merli,[25] L. Meyer Garcia,[2] D. Miao,[4,6] H. Miao,[6] M. Mikhasenko,[71,t] D. A. Milanes,[70] E. Millard,[51] M. Milovanovic,[43] M.-N. Minard,[8,a] A. Minotti,[26,f] E. Minucci,[63] T. Miralles,[9] S. E. Mitchell,[53] B. Mitreska,[15] D. S. Mitzel,[15] A. Modak,[52] A. Mödden,[15] R. A. Mohammed,[58] R. D. Moise,[14] S. Mokhnenko,[38] T. Mombächer,[41] M. Monk,[51,64] I. A. Monroy,[70] S. Monteil,[9] G. Morello,[23] M. J. Morello,[29,d] M. P. Morgenthaler,[17] J. Moron,[34] A. B. Morris,[43] A. G. Morris,[10] R. Mountain,[63] H. Mu,[3] E. Muhammad,[51] F. Muheim,[53] M. Mulder,[74] K. Müller,[45] C. H. Murphy,[58] D. Murray,[57] R. Murta,[56] P. Muzzetto,[27,k] P. Naik,[49] T. Nakada,[44] R. Nandakumar,[52] T. Nanut,[43] I. Nasteva,[2] M. Needham,[53] N. Neri,[25,m] S. Neubert,[71] N. Neufeld,[43] P. Neustroev,[38] R. Newcombe,[56] J. Nicolini,[15,11] D. Nicotra,[75] E. M. Niel,[44] S. Nieswand,[14] N. Nikitin,[38] N. S. Nolte,[59] C. Normand,[8,27,k] J. Novoa Fernandez,[41] G. N Nowak,[60] C. Nunez,[78] A. Oblakowska-Mucha,[34] V. Obraztsov,[38] T. Oeser,[14] S. Okamura,[21,e] R. Oldeman,[27,k] F. Oliva,[53] C. J. G. Onderwater,[74] R. H. O'Neil,[53] J. M. Otalora Goicochea,[2] T. Ovsiannikova,[38] P. Owen,[45] A. Oyanguren,[42] O. Ozcelik,[53] K. O. Padeken,[71] B. Pagare,[51] P. R. Pais,[43] T. Pajero,[58] A. Palano,[19] M. Palutan,[23] G. Panshin,[38] L. Paolucci,[51] A. Papanestis,[52] M. Pappagallo,[19,j] L. L. Pappalardo,[21,e] C. Pappenheimer,[60] W. Parker,[61] C. Parkes,[57] B. Passalacqua,[21] G. Passaleva,[22] A. Pastore,[19] M. Patel,[56] C. Patrignani,[20,g] C. J. Pawley,[75] A. Pellegrino,[32] M. Pepe Altarelli,[43] S. Perazzini,[20] D. Pereima,[38] A. Pereiro Castro,[41] P. Perret,[9] K. Petridis,[49] A. Petrolini,[24,h] S. Petrucci,[53] M. Petruzzo,[25] H. Pham,[63] A. Philippov,[38] R. Piandani,[6] L. Pica,[29,d] M. Piccini,[73] B. Pietrzyk,[8] G. Pietrzyk,[11] M. Pili,[58] D. Pinci,[30] F. Pisani,[43] M. Pizzichemi,[26,43,f] V. Placinta,[37] J. Plews,[48] M. Plo Casasus,[41] F. Polci,[13,43] M. Poli Lener,[23] A. Poluektov,[10] N. Polukhina,[38] I. Polyakov,[43] E. Polycarpo,[2] S. Ponce,[43] D. Popov,[6,43] S. Poslavskii,[38] K. Prasanth,[35] L. Promberger,[17] C. Prouve,[41] V. Pugatch,[47] V. Puill,[11] G. Punzi,[29,p] H. R. Qi,[3] W. Qian,[6] N. Qin,[3] S. Qu,[3] R. Quagliani,[44] N. V. Raab,[18] B. Rachwal,[34] J. H. Rademacker,[49] R. Rajagopalan,[63] M. Rama,[29] M. Ramos Pernas,[51] M. S. Rangel,[2] F. Ratnikov,[38] G. Raven,[33] M. Rebollo De Miguel,[42] F. Redi,[43] J. Reich,[49] F. Reiss,[57] C. Remon Alepuz,[42] Z. Ren,[3] P. K. Resmi,[58] R. Ribatti,[29,d] A. M. Ricci,[27] S. Ricciardi,[52] K. Richardson,[59] M. Richardson-Slipper,[53] K. Rinnert,[55] P. Robbe,[11] G. Robertson,[53] E. Rodrigues,[55,43] E. Rodriguez Fernandez,[41] J. A. Rodriguez Lopez,[70] E. Rodriguez Rodriguez,[41] D. L. Rolf,[43] A. Rollings,[58] P. Roloff,[43] V. Romanovskiy,[38] M. Romero Lamas,[41] A. Romero Vidal,[41] J. D. Roth,[78,a] M. Rotondo,[23] M. S. Rudolph,[63] T. Ruf,[43] R. A. Ruiz Fernandez,[41] J. Ruiz Vidal,[42] A. Ryzhikov,[38] J. Ryzka,[34] J. J. Saborido Silva,[41] N. Sagidova,[38] N. Sahoo,[48] B. Saitta,[27,k] M. Salomoni,[43] C. Sanchez Gras,[32] I. Sanderswood,[42] R. Santacesaria,[30] C. Santamarina Rios,[41] M. Santimaria,[23] L. Santoro,[1] E. Santovetti,[31,b] D. Saranin,[38] G. Sarpis,[53] M. Sarpis,[71] A. Sarti,[30] C. Satriano,[30,u] A. Satta,[31] M. Saur,[5] D. Savrina,[38] H. Sazak,[9] L. G. Scantlebury Smead,[58] A. Scarabotto,[13] S. Schael,[14] S. Scherl,[55] A. M. Schertz,[72] M. Schiller,[54] H. Schindler,[43] M. Schmelling,[16] B. Schmidt,[43] S. Schmitt,[14] O. Schneider,[44] A. Schopper,[43] M. Schubiger,[32] N. Schulte,[15] S. Schulte,[44] M. H. Schune,[11] R. Schwemmer,[43] B. Sciascia,[23] A. Sciuccati,[43] S. Sellam,[41] A. Semennikov,[38] M. Senghi Soares,[33] A. Sergi,[24,h] N. Serra,[45] L. Sestini,[28] A. Seuthe,[15] Y. Shang,[5] D. M. Shangase,[78] M. Shapkin,[38] I. Shchemerov,[38] L. Shchutska,[44] T. Shears,[55] L. Shekhtman,[38] Z. Shen,[5] S. Sheng,[4,6] V. Shevchenko,[38] B. Shi,[6] E. B. Shields,[26,f] Y. Shimizu,[11] E. Shmanin,[38] R. Shorkin,[38] J. D. Shupperd,[63] B. G. Siddi,[21,e] R. Silva Coutinho,[63] G. Simi,[28] S. Simone,[19,j] M. Singla,[64] N. Skidmore,[57] R. Skuza,[17] T. Skwarnicki,[63] M. W. Slater,[48] J. C. Smallwood,[58] J. G. Smeaton,[50] E. Smith,[45] K. Smith,[62] M. Smith,[56] A. Snoch,[32] L. Soares Lavra,[9] M. D. Sokoloff,[60] F. J. P. Soler,[54] A. Solomin,[38,49] A. Solovev,[38]

I. Solovyev,[38] R. Song,[64] F. L. Souza De Almeida,[2] B. Souza De Paula,[2] B. Spaan,[15,a] E. Spadaro Norella,[25,m] E. Spedicato,[20] J. G. Speer,[15] E. Spiridenkov,[38] P. Spradlin,[54] V. Sriskaran,[43] F. Stagni,[43] M. Stahl,[43] S. Stahl,[43] S. Stanislaus,[58] E. N. Stein,[43] O. Steinkamp,[45] O. Stenyakin,[38] H. Stevens,[15] D. Strekalina,[38] Y. S Su,[6] F. Suljik,[58] J. Sun,[27] L. Sun,[69] Y. Sun,[61] P. N. Swallow,[48] K. Swientek,[34] A. Szabelski,[36] T. Szumlak,[34] M. Szymanski,[43] Y. Tan,[3] S. Taneja,[57] M. D. Tat,[58] A. Terentev,[45] F. Teubert,[43] E. Thomas,[43] D. J. D. Thompson,[48] H. Tilquin,[56] V. Tisserand,[9] S. T'Jampens,[8] M. Tobin,[4] L. Tomassetti,[21,e] G. Tonani,[25,m] X. Tong,[5] D. Torres Machado,[1] D. Y. Tou,[3] C. Trippl,[44] G. Tuci,[6] N. Tuning,[32] A. Ukleja,[36] D. J. Unverzagt,[17] A. Usachov,[33] A. Ustyuzhanin,[38] U. Uwer,[17] V. Vagnoni,[20] A. Valassi,[43] G. Valenti,[20] N. Valls Canudas,[39] M. Van Dijk,[44] H. Van Hecke,[62] E. van Herwijnen,[56] C. B. Van Hulse,[41,v] M. van Veghel,[32] R. Vazquez Gomez,[40] P. Vazquez Regueiro,[41] C. Vázquez Sierra,[41] S. Vecchi,[21] J. J. Velthuis,[49] M. Veltri,[22,w] A. Venkateswaran,[44] M. Veronesi,[32] M. Vesterinen,[51] D. Vieira,[60] M. Vieites Diaz,[44] X. Vilasis-Cardona,[39] E. Vilella Figueras,[55] A. Villa,[20] P. Vincent,[13] F. C. Volle,[11] D. vom Bruch,[10] V. Vorobyev,[38] N. Voropaev,[38] K. Vos,[75] C. Vrahas,[53] J. Walsh,[29] E. J. Walton,[64] G. Wan,[5] C. Wang,[17] G. Wang,[7] J. Wang,[5] J. Wang,[4] J. Wang,[3] J. Wang,[69] M. Wang,[25] R. Wang,[49] X. Wang,[67] Y. Wang,[7] Z. Wang,[45] Z. Wang,[3] Z. Wang,[6] J. A. Ward,[51,64] N. K. Watson,[48] D. Websdale,[56] Y. Wei,[5] B. D. C. Westhenry,[49] D. J. White,[57] M. Whitehead,[54] A. R. Wiederhold,[51] D. Wiedner,[15] G. Wilkinson,[58] M. K. Wilkinson,[60] I. Williams,[50] M. Williams,[59] M. R. J. Williams,[53] R. Williams,[50] F. F. Wilson,[52] W. Wislicki,[36] M. Witek,[35] L. Witola,[17] C. P. Wong,[62] G. Wormser,[11] S. A. Wotton,[50] H. Wu,[63] J. Wu,[7] K. Wyllie,[43] Z. Xiang,[6] Y. Xie,[7] A. Xu,[5] J. Xu,[6] L. Xu,[3] L. Xu,[3] M. Xu,[51] Q. Xu,[6] Z. Xu,[9] Z. Xu,[6] D. Yang,[3] S. Yang,[6] X. Yang,[5] Y. Yang,[6] Z. Yang,[5] Z. Yang,[61] L. E. Yeomans,[55] V. Yeroshenko,[11] H. Yeung,[57] H. Yin,[7] J. Yu,[66] X. Yuan,[63] E. Zaffaroni,[44] M. Zavertyaev,[16] M. Zdybal,[35] M. Zeng,[3] C. Zhang,[5] D. Zhang,[7] J. Zhang,[6] L. Zhang,[3] S. Zhang,[66] S. Zhang,[5] Y. Zhang,[5] Y. Zhang,[58] Y. Zhao,[17] A. Zharkova,[38] A. Zhelezov,[17] Y. Zheng,[6] T. Zhou,[5] X. Zhou,[7] Y. Zhou,[6] V. Zhovkovska,[11] X. Zhu,[3] X. Zhu,[7] Z. Zhu,[6] V. Zhukov,[14,38] J. Zhuo,[42] Q. Zou,[4,6] S. Zucchelli,[20,g] D. Zuliani,[28] and G. Zunica[57]

(LHCb Collaboration)

[1]*Centro Brasileiro de Pesquisas Físicas (CBPF), Rio de Janeiro, Brazil*
[2]*Universidade Federal do Rio de Janeiro (UFRJ), Rio de Janeiro, Brazil*
[3]*Center for High Energy Physics, Tsinghua University, Beijing, China*
[4]*Institute of High Energy Physics (IHEP), Beijing, China*
[5]*School of Physics State Key Laboratory of Nuclear Physics and Technology, Peking University, Beijing, China*
[6]*University of Chinese Academy of Sciences, Beijing, China*
[7]*Institute of Particle Physics, Central China Normal University, Wuhan, Hubei, China*
[8]*Université Savoie Mont Blanc, CNRS, IN2P3-LAPP, Annecy, France*
[9]*Université Clermont Auvergne, CNRS/IN2P3, LPC, Clermont-Ferrand, France*
[10]*Aix Marseille Université, CNRS/IN2P3, CPPM, Marseille, France*
[11]*Université Paris-Saclay, CNRS/IN2P3, IJCLab, Orsay, France*
[12]*Laboratoire Leprince-Ringuet, CNRS/IN2P3, Ecole Polytechnique, Institut Polytechnique de Paris, Palaiseau, France*
[13]*LPNHE, Sorbonne Université, Paris Diderot Sorbonne Paris Cité, CNRS/IN2P3, Paris, France*
[14]*I. Physikalisches Institut, RWTH Aachen University, Aachen, Germany*
[15]*Fakultät Physik, Technische Universität Dortmund, Dortmund, Germany*
[16]*Max-Planck-Institut für Kernphysik (MPIK), Heidelberg, Germany*
[17]*Physikalisches Institut, Ruprecht-Karls-Universität Heidelberg, Heidelberg, Germany*
[18]*School of Physics, University College Dublin, Dublin, Ireland*
[19]*INFN Sezione di Bari, Bari, Italy*
[20]*INFN Sezione di Bologna, Bologna, Italy*
[21]*INFN Sezione di Ferrara, Ferrara, Italy*
[22]*INFN Sezione di Firenze, Firenze, Italy*
[23]*INFN Laboratori Nazionali di Frascati, Frascati, Italy*
[24]*INFN Sezione di Genova, Genova, Italy*
[25]*INFN Sezione di Milano, Milano, Italy*

[26]INFN Sezione di Milano-Bicocca, Milano, Italy
[27]INFN Sezione di Cagliari, Monserrato, Italy
[28]Università degli Studi di Padova, Università e INFN, Padova, Italy
[29]INFN Sezione di Pisa, Pisa, Italy
[30]INFN Sezione di Roma La Sapienza, Roma, Italy
[31]INFN Sezione di Roma Tor Vergata, Roma, Italy
[32]Nikhef National Institute for Subatomic Physics, Amsterdam, Netherlands
[33]Nikhef National Institute for Subatomic Physics and VU University Amsterdam, Amsterdam, Netherlands
[34]AGH—University of Science and Technology,
Faculty of Physics and Applied Computer Science, Kraków, Poland
[35]Henryk Niewodniczanski Institute of Nuclear Physics Polish Academy of Sciences, Kraków, Poland
[36]National Center for Nuclear Research (NCBJ), Warsaw, Poland
[37]Horia Hulubei National Institute of Physics and Nuclear Engineering, Bucharest-Magurele, Romania
[38]Affiliated with an institute covered by a cooperation agreement with CERN
[39]DS4DS, La Salle, Universitat Ramon Llull, Barcelona, Spain
[40]ICCUB, Universitat de Barcelona, Barcelona, Spain
[41]Instituto Galego de Física de Altas Enerxías (IGFAE), Universidade de Santiago de Compostela,
Santiago de Compostela, Spain
[42]Instituto de Fisica Corpuscular, Centro Mixto Universidad de Valencia—CSIC, Valencia, Spain
[43]European Organization for Nuclear Research (CERN), Geneva, Switzerland
[44]Institute of Physics, Ecole Polytechnique Fédérale de Lausanne (EPFL), Lausanne, Switzerland
[45]Physik-Institut, Universität Zürich, Zürich, Switzerland
[46]NSC Kharkiv Institute of Physics and Technology (NSC KIPT), Kharkiv, Ukraine
[47]Institute for Nuclear Research of the National Academy of Sciences (KINR), Kyiv, Ukraine
[48]University of Birmingham, Birmingham, United Kingdom
[49]H.H. Wills Physics Laboratory, University of Bristol, Bristol, United Kingdom
[50]Cavendish Laboratory, University of Cambridge, Cambridge, United Kingdom
[51]Department of Physics, University of Warwick, Coventry, United Kingdom
[52]STFC Rutherford Appleton Laboratory, Didcot, United Kingdom
[53]School of Physics and Astronomy, University of Edinburgh, Edinburgh, United Kingdom
[54]School of Physics and Astronomy, University of Glasgow, Glasgow, United Kingdom
[55]Oliver Lodge Laboratory, University of Liverpool, Liverpool, United Kingdom
[56]Imperial College London, London, United Kingdom
[57]Department of Physics and Astronomy, University of Manchester, Manchester, United Kingdom
[58]Department of Physics, University of Oxford, Oxford, United Kingdom
[59]Massachusetts Institute of Technology, Cambridge, Massachusetts, USA
[60]University of Cincinnati, Cincinnati, Ohio, USA
[61]University of Maryland, College Park, Maryland, USA
[62]Los Alamos National Laboratory (LANL), Los Alamos, New Mexico, USA
[63]Syracuse University, Syracuse, New York, USA
[64]School of Physics and Astronomy, Monash University, Melbourne, Australia (associated with
Department of Physics, University of Warwick, Coventry, United Kingdom)
[65]Pontifícia Universidade Católica do Rio de Janeiro (PUC-Rio), Rio de Janeiro, Brazil (associated with
Universidade Federal do Rio de Janeiro (UFRJ), Rio de Janeiro, Brazil)
[66]Physics and Micro Electronic College, Hunan University, Changsha City, China (associated with
Institute of Particle Physics, Central China Normal University, Wuhan, Hubei, China)
[67]Guangdong Provincial Key Laboratory of Nuclear Science, Guangdong-Hong Kong Joint Laboratory of
Quantum Matter, Institute of Quantum Matter, South China Normal University, Guangzhou, China
(associated with Center for High Energy Physics, Tsinghua University, Beijing, China)
[68]Lanzhou University, Lanzhou, China (associated with Institute of High Energy Physics (IHEP),
Beijing, China)
[69]School of Physics and Technology, Wuhan University, Wuhan, China (associated with Center for High
Energy Physics, Tsinghua University, Beijing, China)
[70]Departamento de Fisica, Universidad Nacional de Colombia, Bogota, Colombia (associated with
LPNHE, Sorbonne Université, Paris Diderot Sorbonne Paris Cité, CNRS/IN2P3, Paris, France)
[71]Universität Bonn—Helmholtz-Institut für Strahlen und Kernphysik, Bonn, Germany (associated with
Physikalisches Institut, Ruprecht-Karls-Universität Heidelberg, Heidelberg, Germany)
[72]Eotvos Lorand University, Budapest, Hungary (associated with European Organization for Nuclear
Research (CERN), Geneva, Switzerland)
[73]INFN Sezione di Perugia, Perugia, Italy (associated with INFN Sezione di Ferrara, Ferrara, Italy)

[74]*Van Swinderen Institute, University of Groningen, Groningen, Netherlands (associated with Nikhef National Institute for Subatomic Physics, Amsterdam, Netherlands)*
[75]*Universiteit Maastricht, Maastricht, Netherlands (associated with Nikhef National Institute for Subatomic Physics, Amsterdam, Netherlands)*
[76]*Faculty of Material Engineering and Physics, Cracow, Poland (associated with Henryk Niewodniczanski Institute of Nuclear Physics Polish Academy of Sciences, Kraków, Poland)*
[77]*Department of Physics and Astronomy, Uppsala University, Uppsala, Sweden (associated with School of Physics and Astronomy, University of Glasgow, Glasgow, United Kingdom)*
[78]*University of Michigan, Ann Arbor, Michigan, USA (associated with Syracuse University, Syracuse, New York, USA)*

[a]Deceased.
[b]Also at Università di Roma Tor Vergata, Roma, Italy.
[c]Also at Università di Firenze, Firenze, Italy.
[d]Also at Scuola Normale Superiore, Pisa, Italy.
[e]Also at Università di Ferrara, Ferrara, Italy.
[f]Also at Università di Milano Bicocca, Milano, Italy.
[g]Also at Università di Bologna, Bologna, Italy.
[h]Also at Università di Genova, Genova, Italy.
[i]Also at Universidad Nacional Autónoma de Honduras, Tegucigalpa, Honduras.
[j]Also at Università di Bari, Bari, Italy.
[k]Also at Università di Cagliari, Cagliari, Italy.
[l]Also at Università di Perugia, Perugia, Italy.
[m]Also at Università degli Studi di Milano, Milano, Italy.
[n]Also at Universidade de Brasília, Brasília, Brazil.
[o]Also at Hangzhou Institute for Advanced Study, UCAS, Hangzhou, China.
[p]Also at Università di Pisa, Pisa, Italy.
[q]Also at Central South University, Changsha, China.
[r]Also at Università di Padova, Padova, Italy.
[s]Also at MSU—Iligan Institute of Technology (MSU-IIT), Iligan, Philippines.
[t]Also at Excellence Cluster ORIGINS, Munich, Germany.
[u]Also at Università della Basilicata, Potenza, Italy.
[v]Also at Universidad de Alcalá, Alcalá de Henares, Spain.
[w]Also at Università di Urbino, Urbino, Italy.